星・惑星系の形成過程 入門

中本泰史 (東工大)

1. 形成過程の概観
2. 分子雲の重力収縮
3. 原始惑星系円盤
4. 固体微粒子の進化
5. 微惑星から惑星へ
6. 惑星系の形成

星間雲・分子雲の状態

星形成領域 (1)

オリオン座

巨大分子雲
距離：1500光年

大質量星・
小質量星が
生まれている

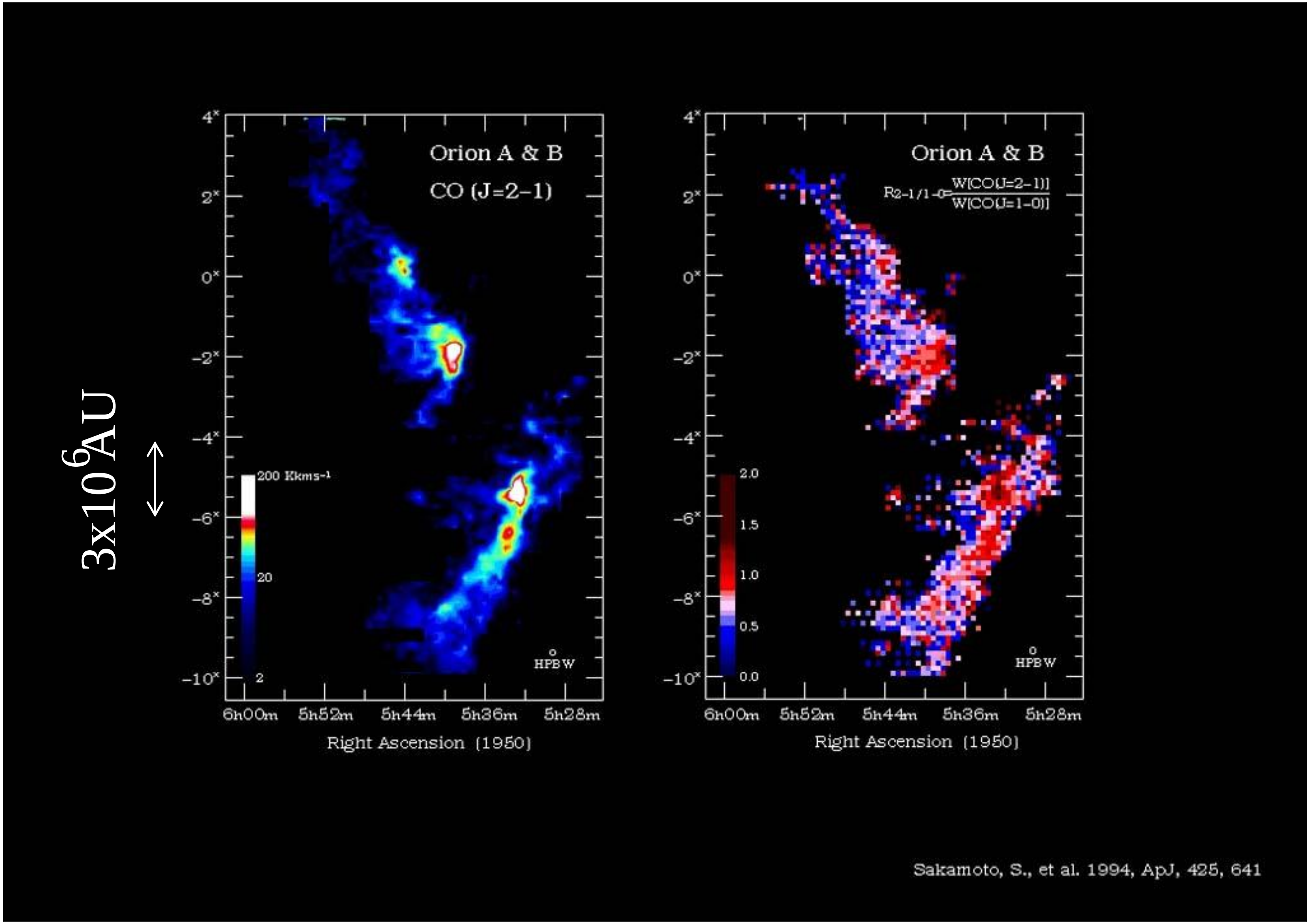
3x10^6AU
Orion A & B
CO (J=2–1)
200 Kkms-1
20
2
HPBW
Right Ascension (1950)
Orion A & B
R2-1/1-0=W[CO(J=2–1)]/W[CO(J=1–0)]
2.0
1.5
1.0
0.5
0.0
HPBW
Right Ascension (1950)
Sakamoto, S., et al. 1994, ApJ, 425, 641

オリオン星雲（阪本他）

星形成領域 (2)

おうし座・ぎょしゃ座

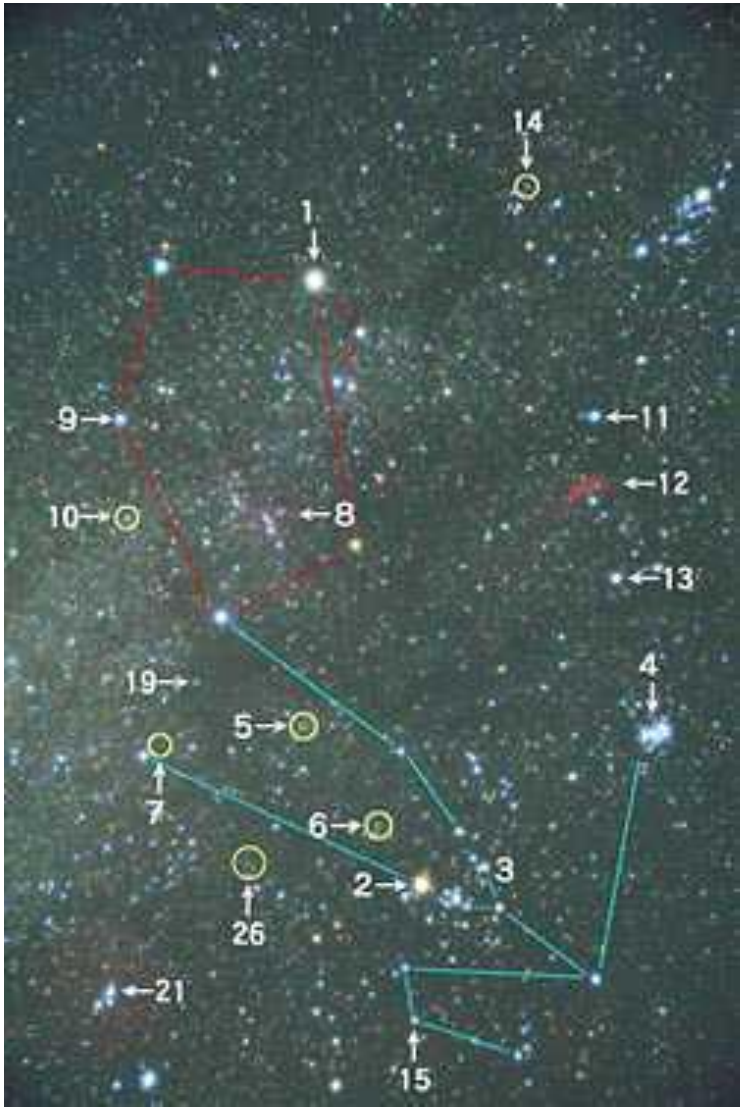

暗黒星雲

距離 140pc

小質量星のみが
生まれている

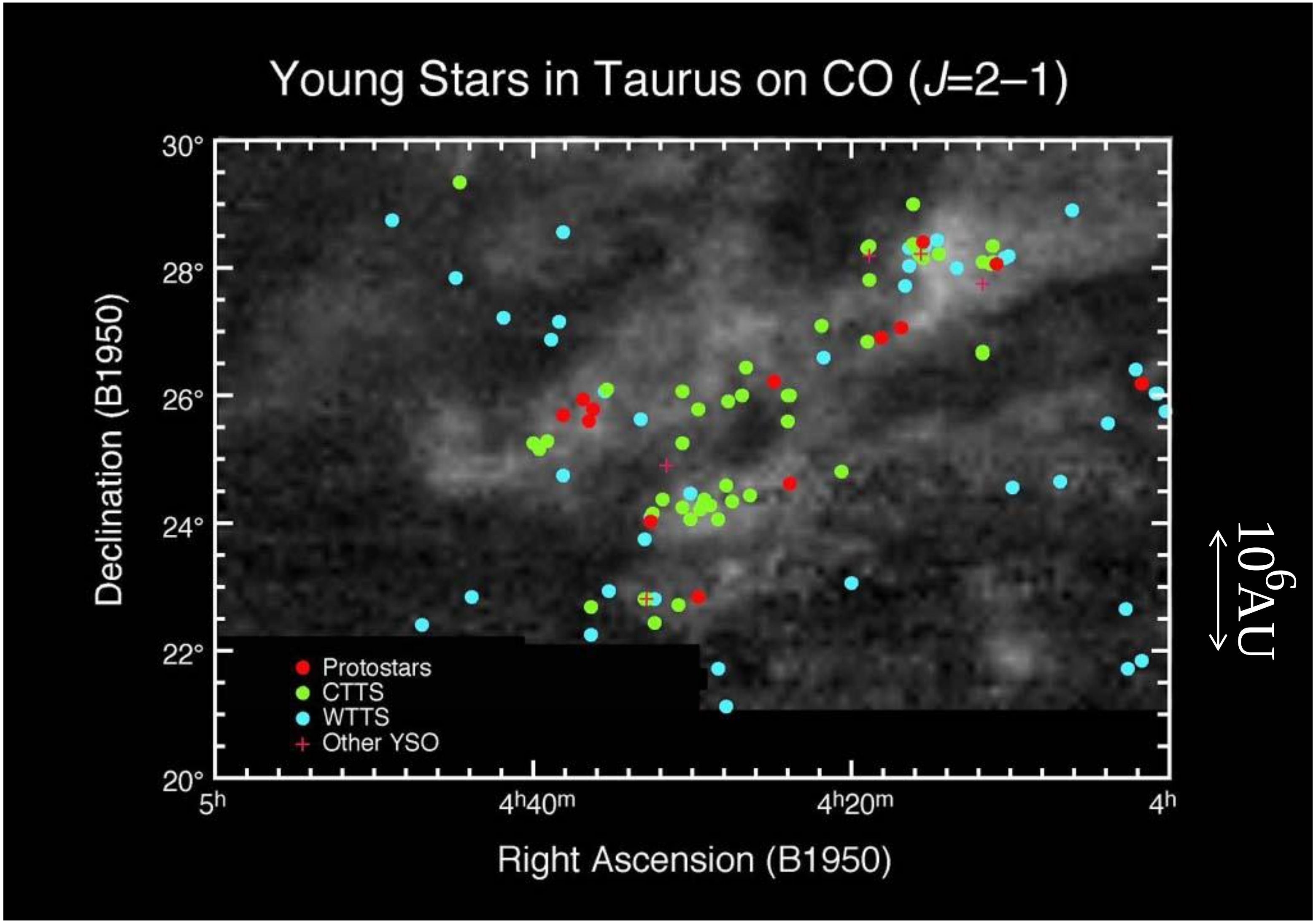

おうし座分子雲：CO(2-1)電波強度
(東大-NRO 60cm)

分子雲

密度：10^3 個 cm^{-3}; H_2, He
温度： 約10K～数十K

加熱：周囲の星からの輻射
宇宙線
冷却：輻射（原子）

分子雲コア

密度：10^5 個 cm^{-3}以上
温度：約10K
サイズ：数万AU

参考：地球大気

密度：3×10^{19} 個 cm^{-3}
温度： 約290K

加熱：太陽からの放射
冷却：宇宙空間への放射

塵

大きさ ~0.1μm = 0.0001 mm

質量：ガスの約 100分の1

数：　水素分子：塵粒子 = 1：10^{-12}

水素分子 10^4個cm^{-3}のとき

塵粒子　10^{-8}個cm^{-3}

参考：黄砂

大きさ ~0.1μm

数　空気分子：黄砂粒子 = 1：10^{-15}

黄砂粒子　10^4個cm^{-3}

渦巻き銀河

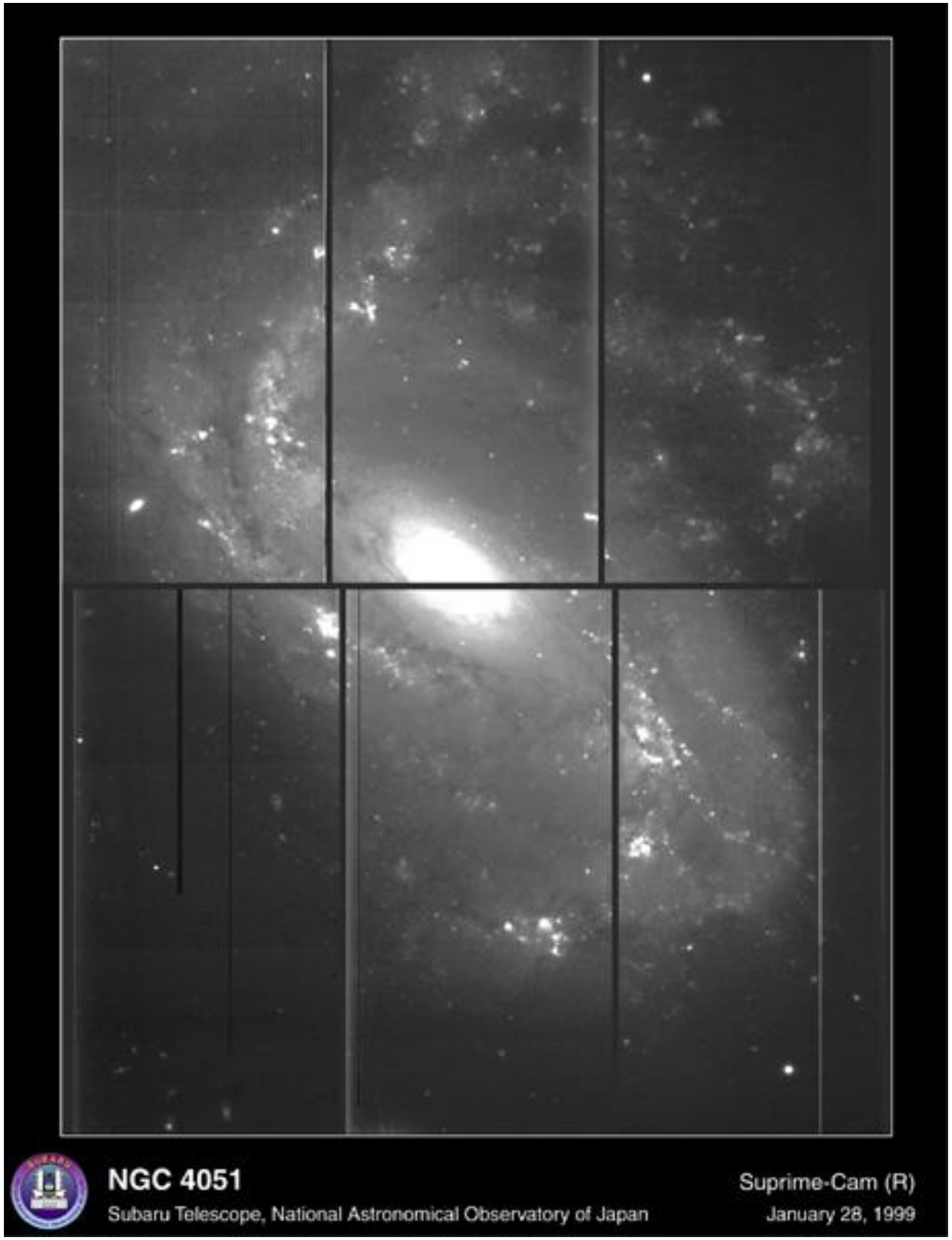
NGC 4051
Subaru Telescope, National Astronomical Observatory of Japan
Suprime-Cam (R)
January 28, 1999

渦巻き銀河
(M64)

Hubble Space Telescope

銀河の構造・星間雲の形成

Baba et al. ApJ (2009)

国立天文台４次元デジタル宇宙プロジェクト提供

分子雲内での星形成

孤立・単独 星形成モード

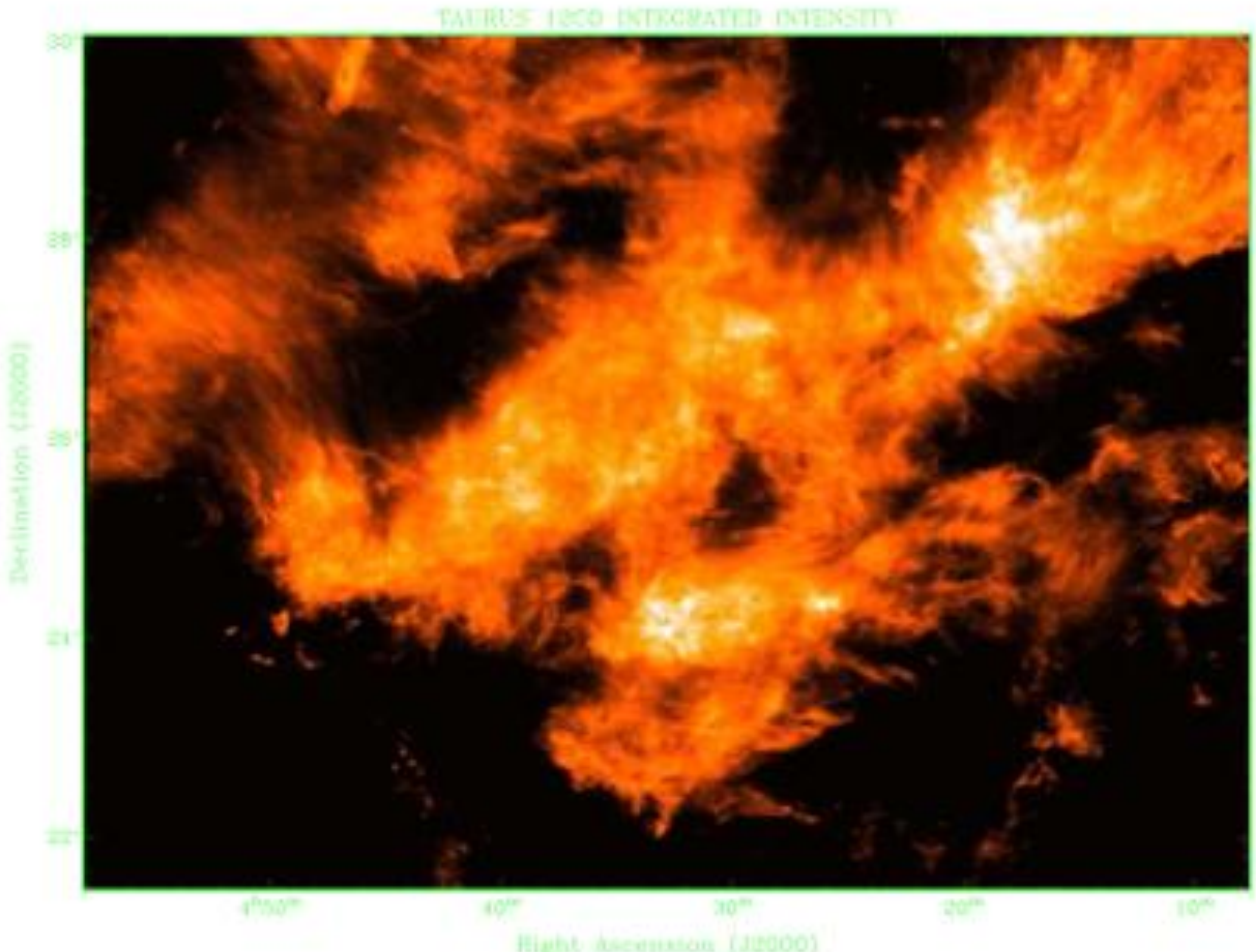

30 pc

おうし座分子雲: ~$10^4 M_\odot$, 星 ~200個, 星形成効率 ~1%

集団的星形成

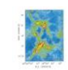

NGC1333

~1pc

~$10^3 M_\odot$

星 ~150個

星形成効率~10%

ほとんどの星は星団で誕生する

(Lada & Lada 03, Allen et al. 07)

1. 多くの分子質量は分子雲にある

2. 分子雲中では，若い星が内部に多く，周辺部に少ない

(例., L1630, Mon OB1, Rosette)

Herschel 望遠鏡による観測結果

Andre et al. 2010

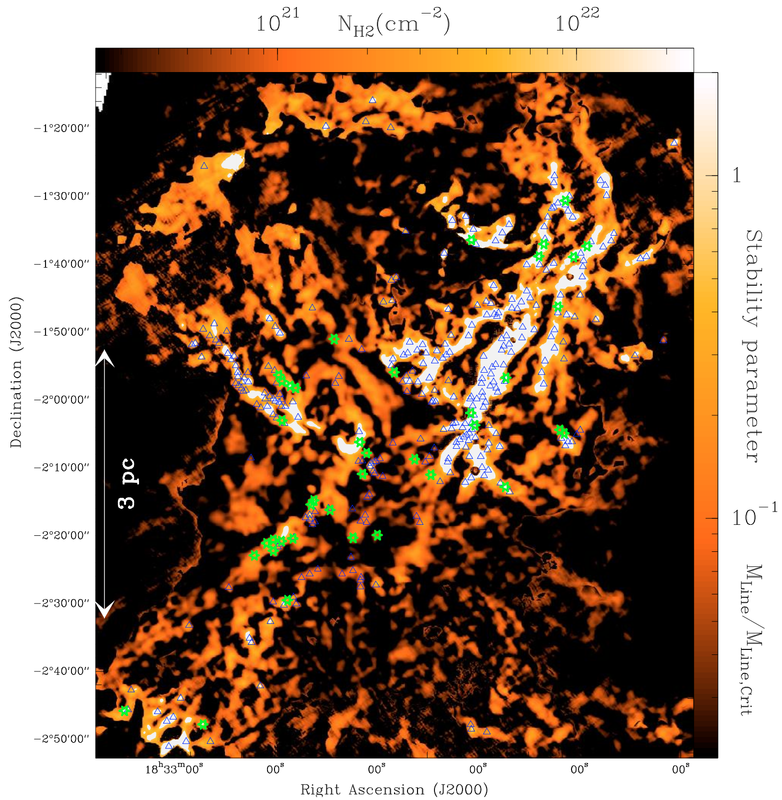

Aquila

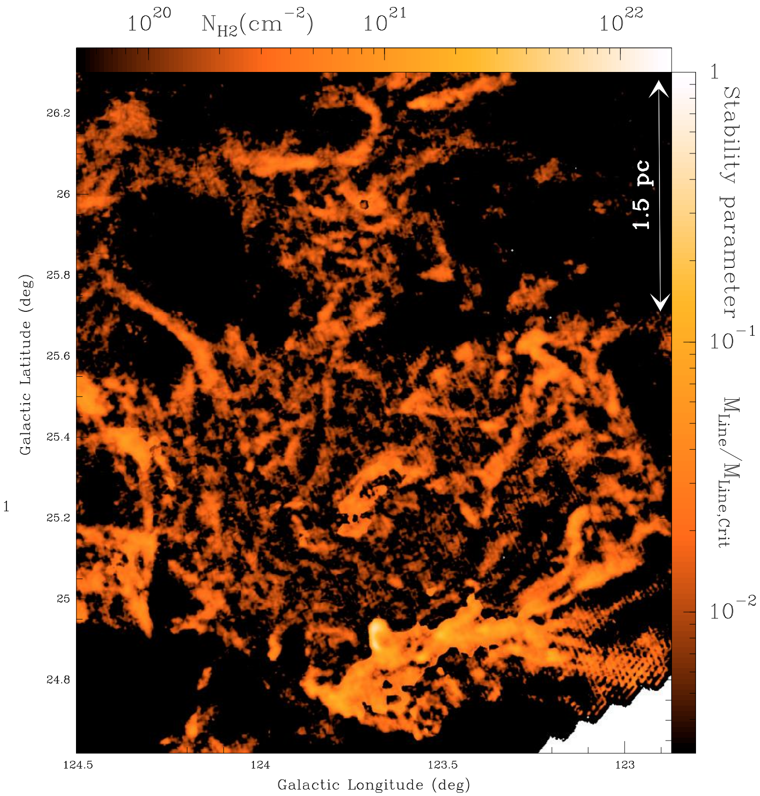

Polaris

Herschel: 70, 100, 160, 500 μm

コアの質量分布

Andre et al. 2010

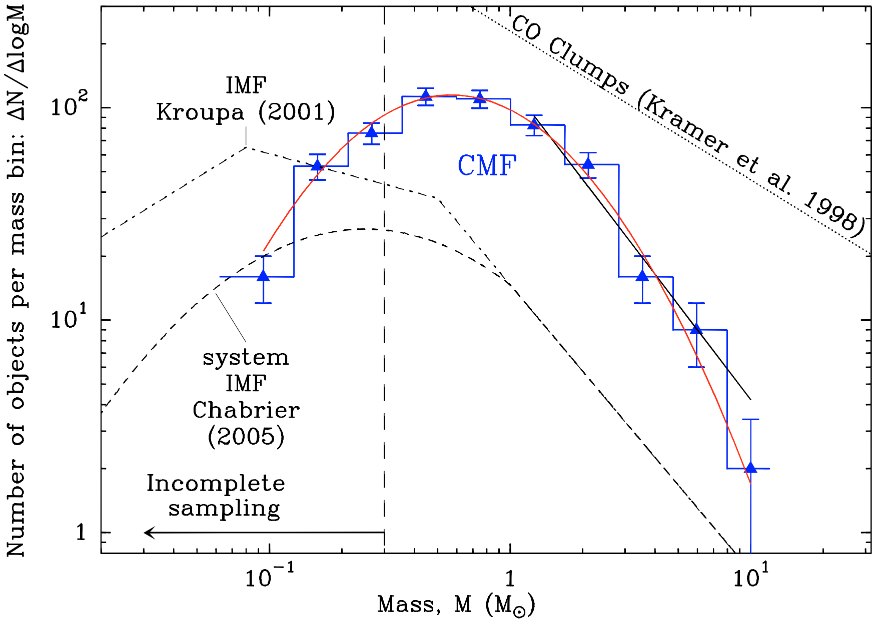

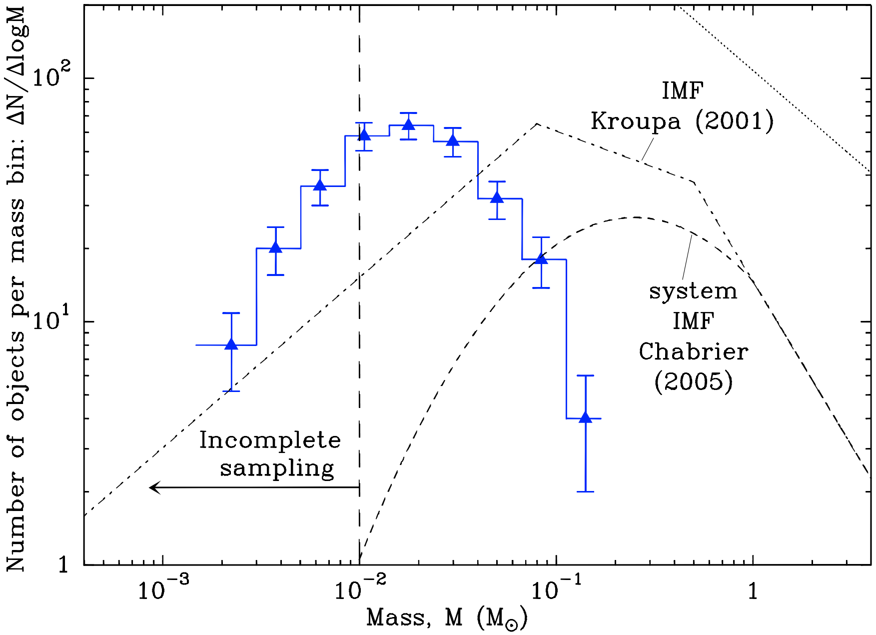

銀河系内の磁場(向き)　可視光偏光観測

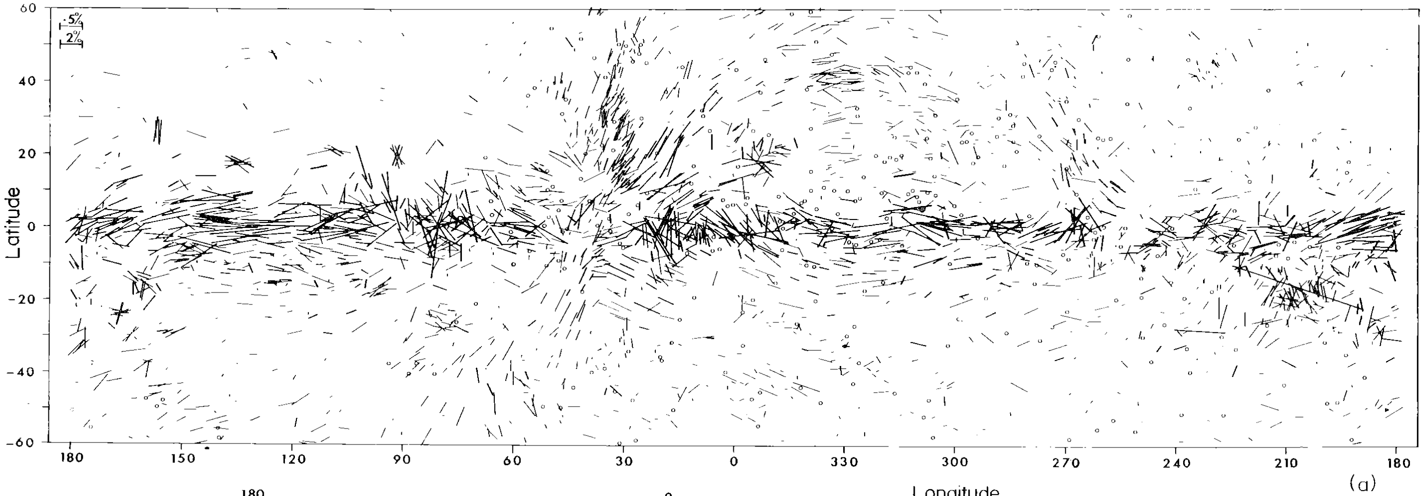

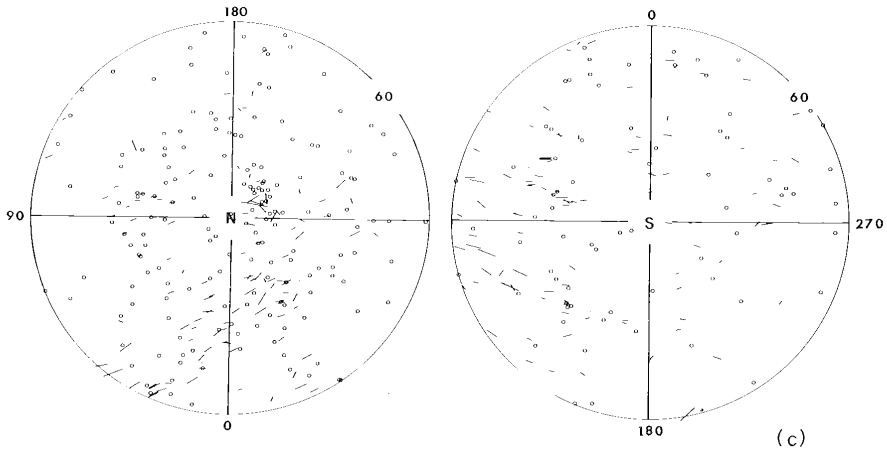

Mathewson & Ford (1970)

星間雲中の磁場強度

Heiles (1982*a*), a very significant new body of Zeeman effect measurements has accumulated which adds to the statistical significance of these data and extends them to regimes of higher density. From these new data, a clearer (although still incomplete) picture of the (B, n) relationship emerges.

II. A COMPILATION OF EXISTING ZEEMAN EFFECT RESULTS

In Figure 1 we present a plot of B versus n which spans more than five orders of magnitude in estimated density and many regimes of the interstellar medium. These regimes include the warm, low-density, partially ionized interstellar gas, diffuse H I shells and clouds, denser H I absorbing regions, and molecular clouds. The figure is similar to Figure 6 of Troland and Heiles (1982*a*), in that all measurements of the field strength and

(1985). Not shown in Figure 1 are ~ 50 upper limits on B derived from H I Zeeman effect results of Heiles. These upper limits are typically $\sim 5\ \mu$G, and they refer to a variety of H I emission regions where densities are mostly in the range 1–50 cm^{-3}.

Finally, the Zeeman-derived field strengths of Figure 1 (except for the rectangular boxes) have all been multiplied by *two.* This procedure accounts for the fact that the Zeeman effect is sensitive to just one component of the magnetic field, and with an *a priori* probability of one-half, the actual field strength in any locale is at least twice the line-of-sight field strength. That is, twice the measured field strength represents a median value since the actual field strength has an equal probability of lying above or below this value.

Zeeman効果を使って測定

Troland & Heiles 1986

experimental conditions, several upper limits an order of magnitude below detected V-amplitudes are derived. In particular, towards W49N due to the source wide velocity coverage and high luminosity, good quality spectra for in total 9 individual velocity features were obtained simultaneously [including limits as low as 6 - 7 mG; five detections with comparable field strength $\langle B_{||} \rangle \sim 40$ mG, one of these reversing field orientation]. Second, as H_2O masers occur in clusters, features closeby in velocity space, coupling differentially to the LHC and RHC beam, may combine to mimic a true Zeeman pattern. For a beam squint of $\sim 1''$ and a maser linewidth of ~ 0.5 km s^{-1}, from modelling synthetic V-spectra we estimate typical amplitudes of $T(V)/T(I) \leq 10^{-3} \cdot \Delta v_r \cdot \Delta \phi_r$. Experimental limits to the relative offsets between the two components in position, $\Delta \phi_r ['']\leq$ a few arcsec, and in velocity, Δv_r [km s^{-1}] < the maser line width,

fields ever *directly* observed in the interstellar medium. These results compare well with constraints from theoretical radiative transfer calculations on the linear polarization characteristics of H_2O supermasers. To explain their often high degree of linear polarization ($Q/I \sim 0.6$ for the 1980 Orion outburst) field strengths, though quite model dependent, of the order of ~ 0.1 G are required (Deguchi and Watson, 1986). From the linear polarization characteristics of the Orion-KL supermaser, Garay et al. (1988) estimate $B \sim 30$ mG, a factor of ~ 2 below our (leakage-limited) upper limit (Table 1, feature at $v \sim 7.4$ km s^{-1}).

There is no direct access to the physical characteristics in the H_2O maser clumps, and the numbers for density and kinetic temperature depend on details of the pump scenario (see Genzel, 1986; Reid and Moran, 1981). In the following, we adopt $n \sim 10^{10 \pm 1}$ cm^{-3}, with the higher densities required for the more

Fiebig & Güsten 1986

エネルギー密度

$$u_m = \frac{B^2}{8\pi} = 4\times 10^{-12}\left(\frac{B}{100\ \mu\mathrm{Gauss}}\right)^2\ \mathrm{erg\ cm^{-3}}$$

$$u_p = \frac{5}{2}nkT = 3.5\times 10^{-12}\left(\frac{n}{10^3\ \mathrm{cm^{-3}}}\right)\left(\frac{T}{10\ \mathrm{K}}\right)\mathrm{erg\ cm^{-3}}$$

$\boxed{u_m > u_p}$

Heiles (1982*a*), a very significant new body of Zeeman effect measurements has accumulated which adds to the statistical significance of these data and extends them to regimes of higher density. From these new data, a clearer (although still incomplete) picture of the (*B*, *n*) relationship emerges.

II. A COMPILATION OF EXISTING ZEEMAN EFFECT RESULTS

In Figure 1 we present a plot of *B* versus *n* which spans more than five orders of magnitude in estimated density and many regimes of the interstellar medium. These regimes include the warm, low-density, partially ionized interstellar gas, diffuse H I shells and clouds, denser H I absorbing regions, and molecular clouds. The figure is similar to Figure 6 of Troland and Heiles (1982*a*), in that all measurements of the field strength and upper limits are derived from the Zeeman effect except for the

(1985). Not shown in Figure 1 are ~50 upper limits on *B* derived from H I Zeeman effect results of Heiles. These upper limits are typically ~5 μG, and they refer to a variety of H I emission regions where densities are mostly in the range 1–50 cm^{-3}.

Finally, the Zeeman-derived field strengths of Figure 1 (except for the rectangular boxes) have all been multiplied by *two.* This procedure accounts for the fact that the Zeeman effect is sensitive to just one component of the magnetic field, and with an *a priori* probability of one-half, the actual field strength in any locale is at least twice the line-of-sight field strength. That is, twice the measured field strength represents a median value since the actual field strength has an equal probability of lying above or below this value.

We have not multiplied the rectangular boxes in Figure 1 by

$\boxed{u_m < u_p}$

Troland & Heiles 1986

超音速乱流 + 磁場

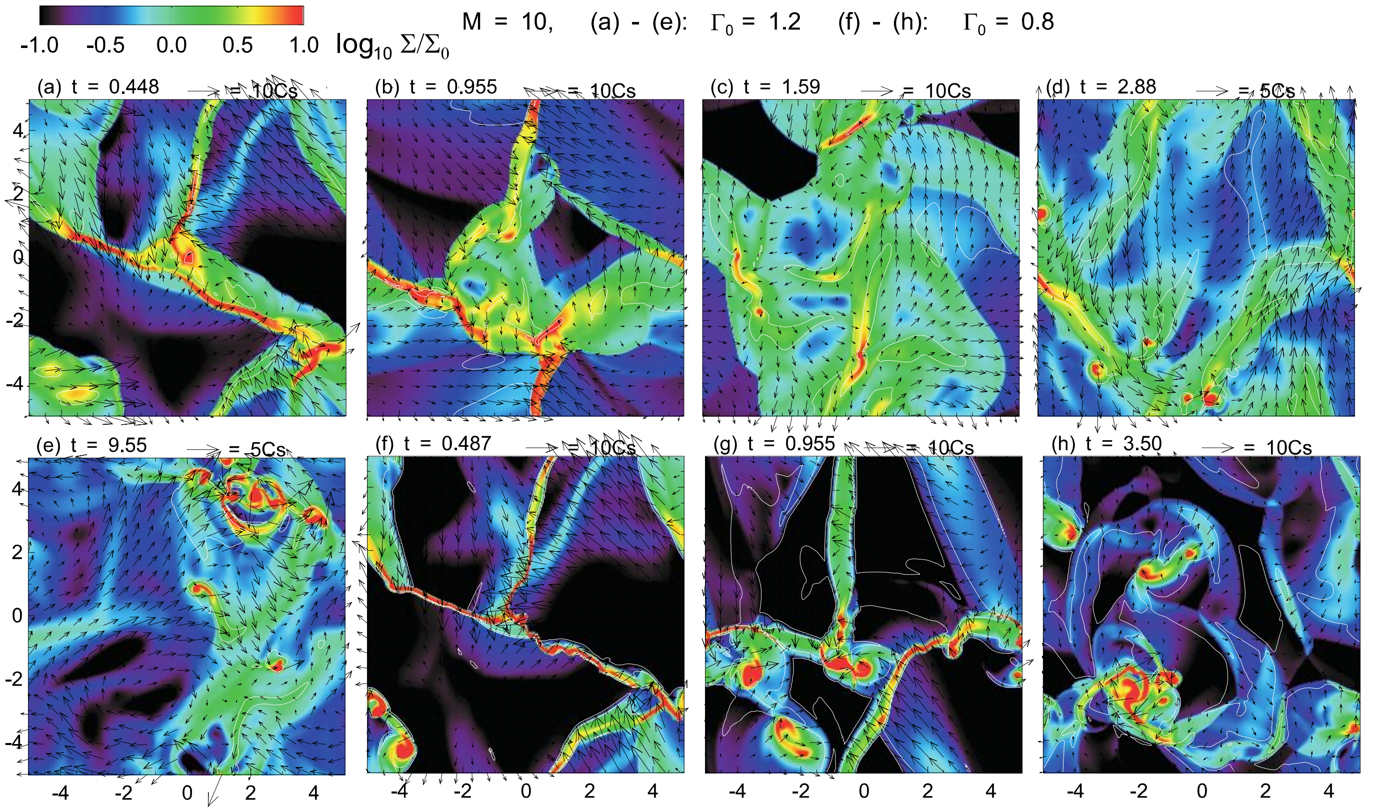

FIG. 1.—Snapshots of magnetized turbulent clouds. (*a–e*) Initially magnetically subcritical cloud with $\Gamma_0 = 1.2$. (*f–h*) Supercritical cloud with $\Gamma_0 = 0.8$. The clouds are stirred at $t = 0$ by the same random velocity field of Mach number $\mathcal{M} = 10$. The color bar is for column density (in units of the initial value Σ_0). The time labeled is in units of the gravitational collapse time t_g, and the length unit is the Jeans length L_J. Shown in each panel are contours of critical flux-to-mass ratio (*in white*) and the velocity field (*in arrows*). The arrow length is proportional to the flow speed, with normalization indicated above the panel.

Li & Nakamura 2004

星間雲

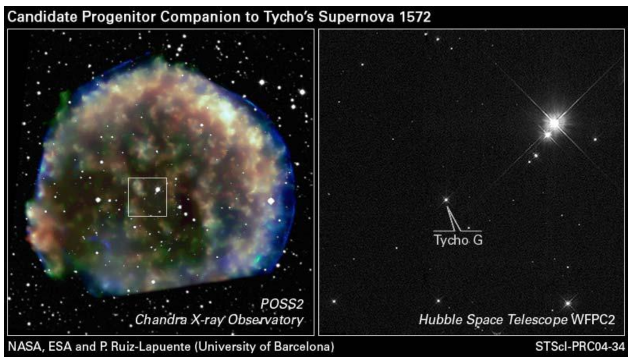

超新星爆発

赤色巨星

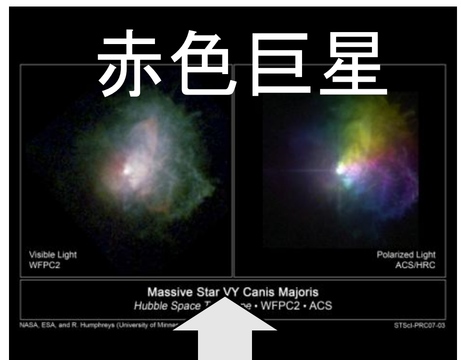

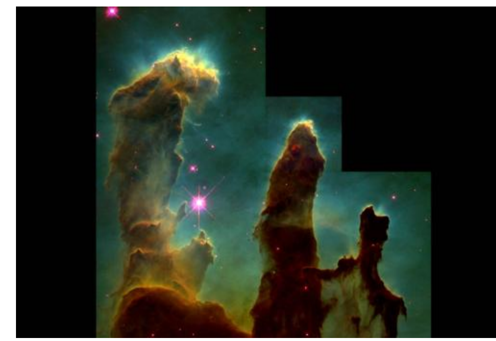

星・惑星系形成

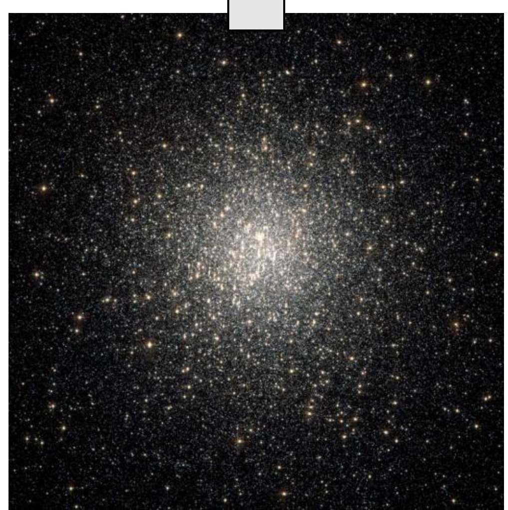

星の進化

Inter Stellar Dust

Matsuura et al. 2011

SN1987Aから放出された物質が固体微粒子になっている

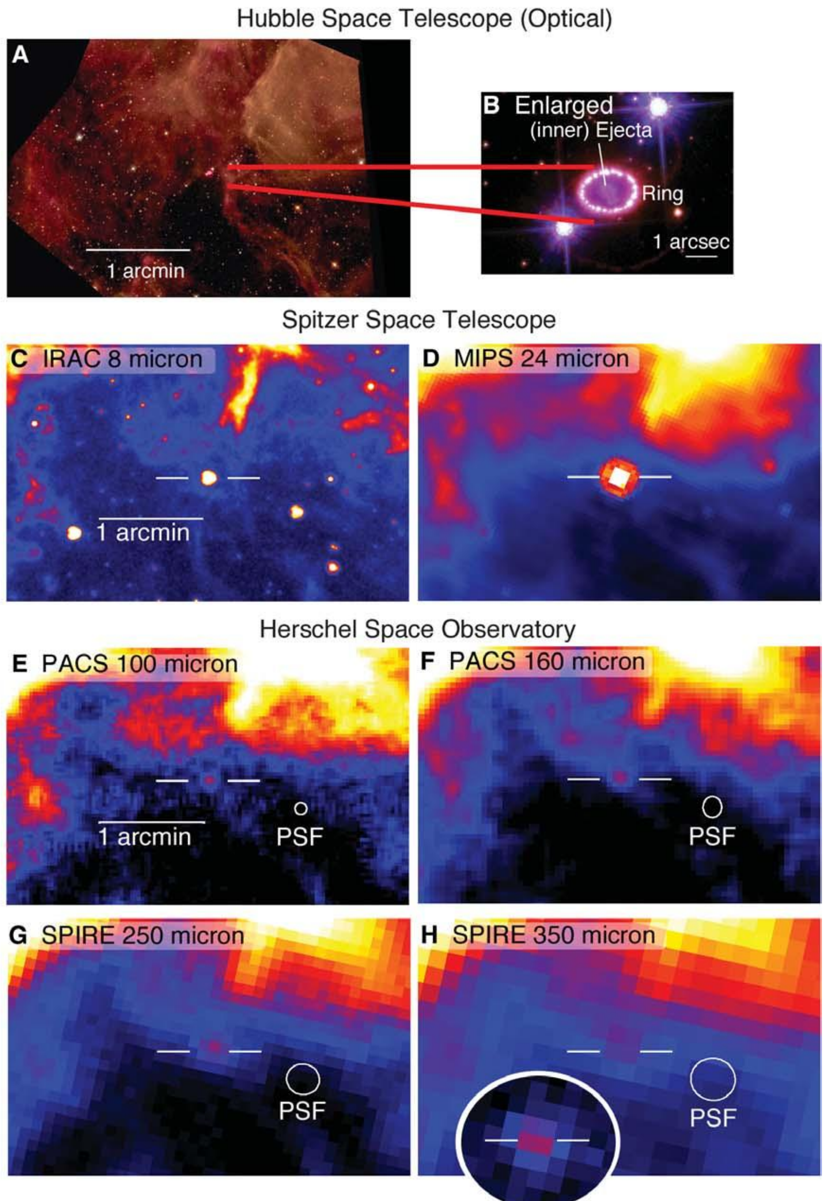

Fig. 1. (**A** to **H**) The Herschel images of SN 1987A, together with the Spitzer infrared (*20*) and the Hubble optical (*56*, *57*) images. North is top, and east is left. The two horizontal white lines indicate the position of SN 1987A measured from radio observations. (**I**) Background-subtracted 350-μm image, where the background is estimated from the 250-μm residual image after the subtraction of the PSF at the position of SN 1987A. The PSFs show the resolution of the Herschel instruments. (B) shows an enlarged HST optical image, indicating the morphology of the SN remnant. [Source: (A) Hubble Heritage Team (Association of Universities for Research in Astronomy (AURA)/Space Telescope Science Institute (STScI)/NASA); (B) NASA, ESA, P. Challis, and R. Kirshner (Harvard-Smithsonian Center for Astrophysics)]

Matsuura et al. 2011

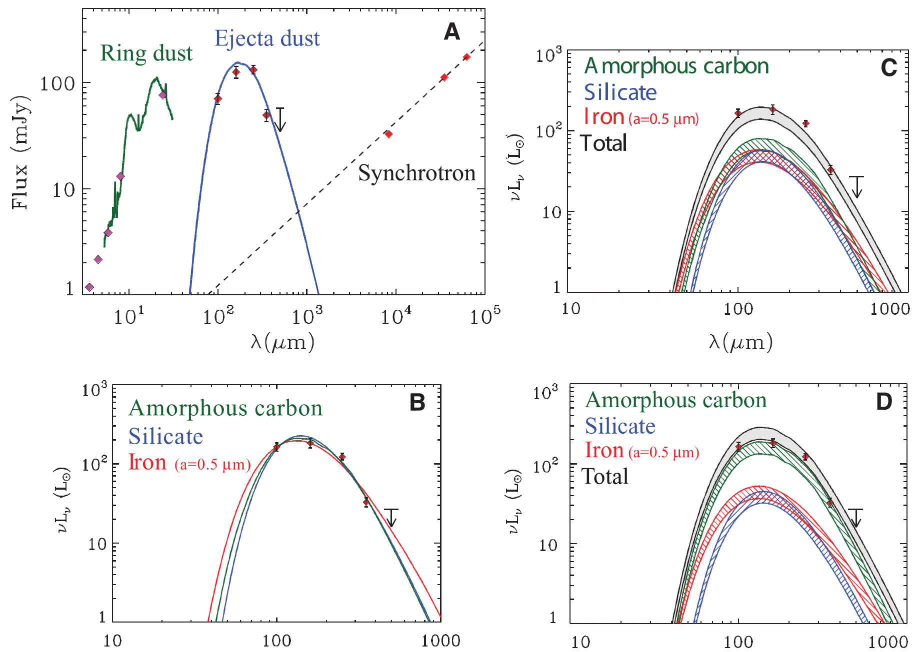

Table 4. The dust mass assumes 100% dust condensation of the available elemental mass (m_d). The range of dust masses reflects the difference in compositions in Table 3. All silicates are assumed to be in the form of MgO and SiO_2 dust. The mass of carbon dust assumes that no substantial fraction of carbon is locked up in CO molecules.

Dust species	m_d ($M_\odot$)	
	Model 1	**Model 2**
Amorphous carbon	0.11	0.26
Silicate	0.52	0.37
Iron	0.08	0.08
Total	0.71	0.71

Molster et al. 2001

赤外線天文衛星(ISO)で
AGB星周りの固体微粒子
を観測

- たくさんある
- 結晶質シリケイトもある

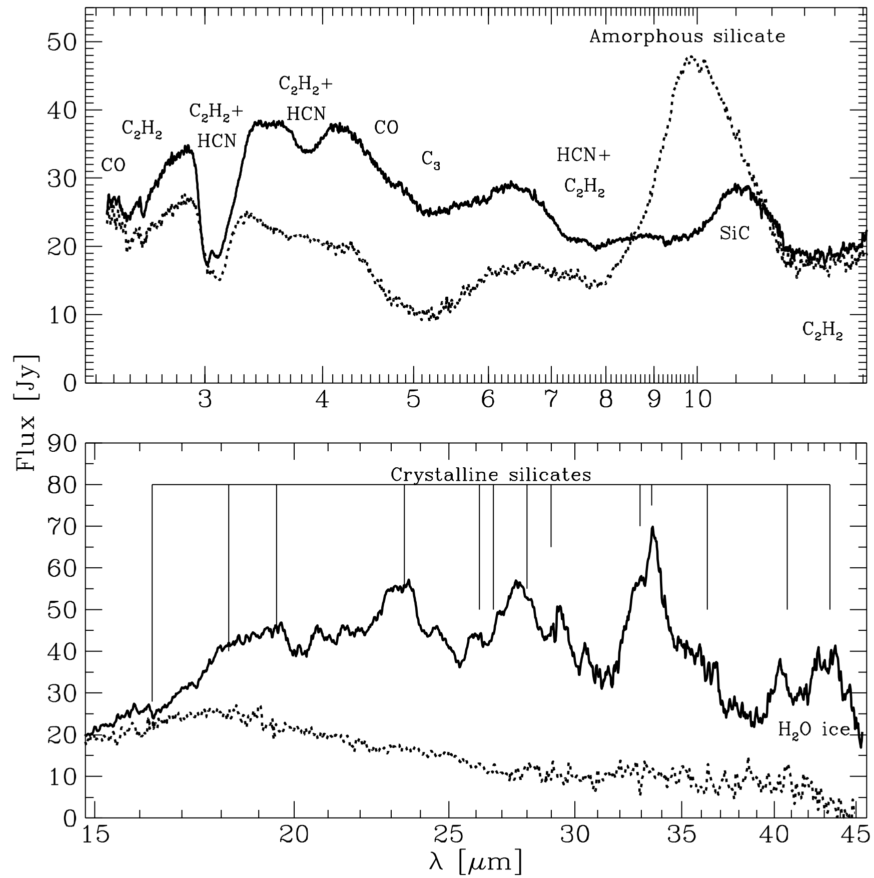

Fig. 1. The SWS spectrum of IRAS 09425−6040 (solid line), compared with the spectrum of a typical silicate carbon star V778 Cyg (dotted line). The spectral features are indicated in the figure

結晶 (水晶)　　　　非晶質 (石英ガラス)

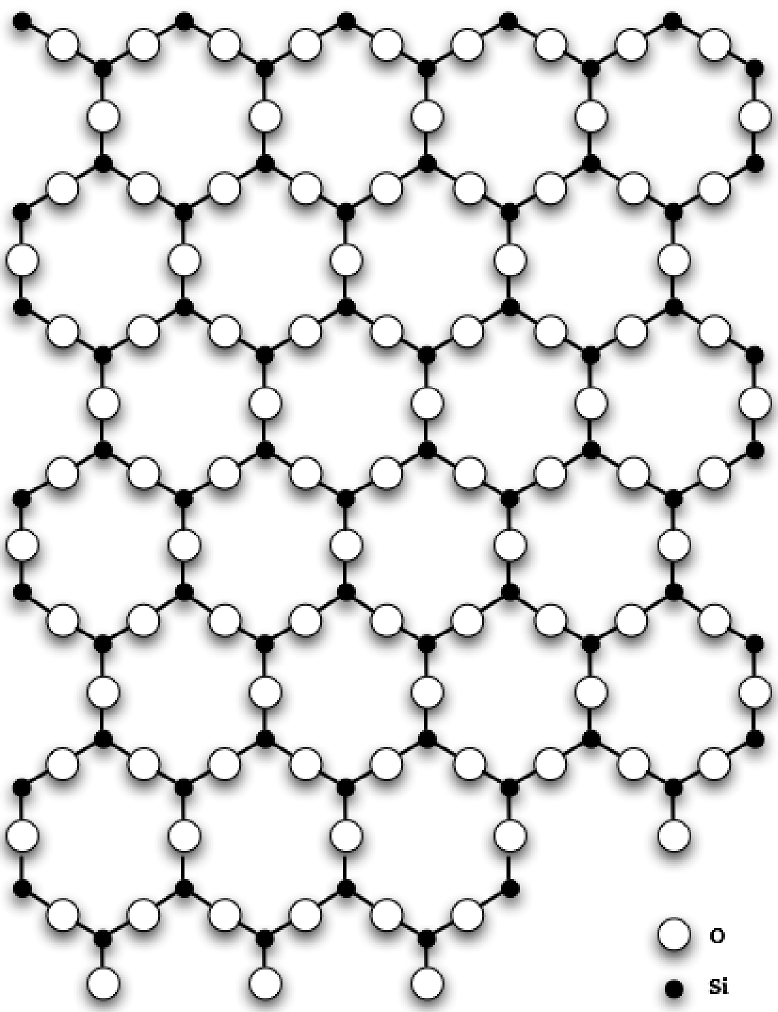

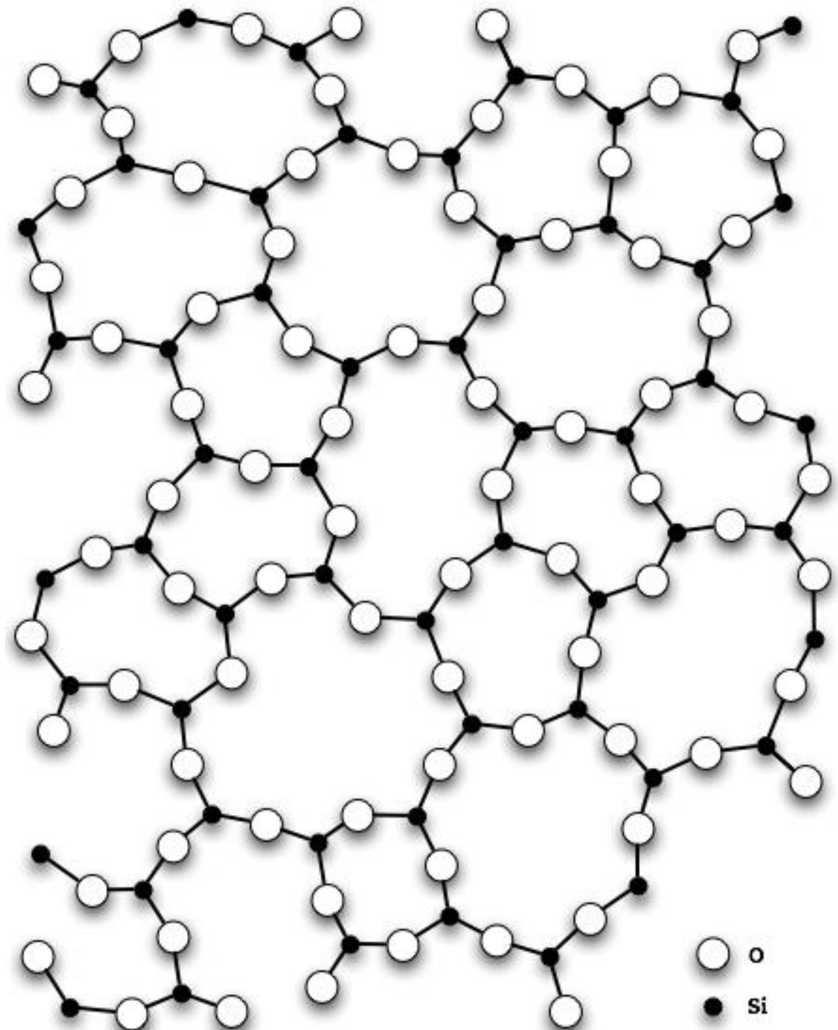

Kemper et al. 2004

赤外線(ISO)で，銀河中心方向の星間ダストのスペクトルを観測

星間ダストのシリケイトで結晶質のもの：
0.2 ± 0.2 %
↓
星間空間には，結晶質の固体微粒子は存在しない

結晶質固体微粒子は，星間空間で，速やかにアモルファス化される

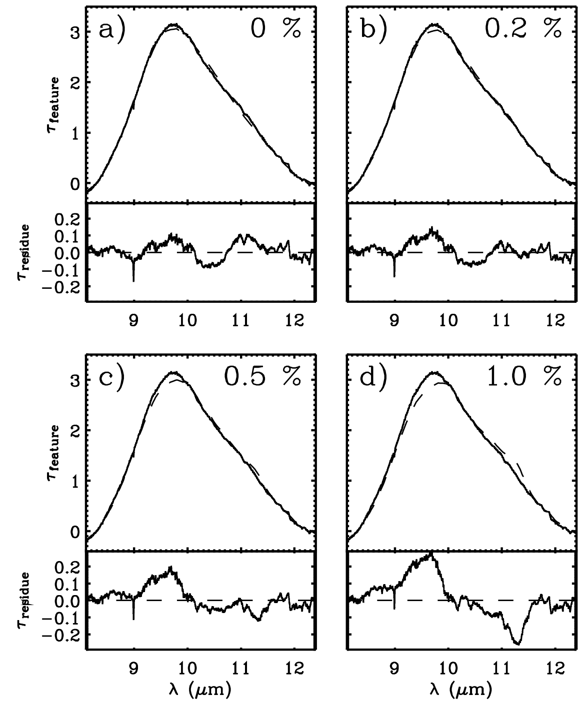

Fig. 4.—Optical depth observed in the 10 μm silicate feature toward Sgr A*. (*a*) The best χ^2 fit consisting of a mixture of amorphous silicates (*dashed line*) to the optical depth in the feature (*solid line*). The lower part of (*a*) shows the residual optical depth after the fit is subtracted from the observed optical depth. (*b–d*) The best χ^2 fit (*dashed line*) to the *ISO* data (*solid line*) of partially crystalline mixtures of silicates with the same ratio of pyroxenes over olivines as in (*a*). In each panel the degree of crystallinity is indicated in the upper right corner, and the lower part of each panel shows the residual optical depth. In the case of the completely amorphous dust composition, the residuals are at most ~3% of the optical depth of the amorphous silicates. The χ^2 values are smallest for the 0.2% degree of crystallinity, which is evident from the residuals as well. With increasing crystallinity, the fit quickly deteriorates, which becomes visible as larger residues. At ~0.5%, the fit is already worse than a completely amorphous composition.

Mathis et al. 1977

紫外線～可視光の
星間吸収　→

星間固体微粒子の
組成とサイズ分布を
推定：MRN モデル

$n(a) \sim a^{-3.5}$
$0.005\ \mu\mathrm{m} < a < 0.25\ \mu\mathrm{m}$

グラファイト + オリビン

NTERSTELLAR GRAINS 429

required for the monotonically decreasing as well as for the single bin distributions. Again, the substance other than graphite shows a smaller range of sizes than the graphite does, but shows about the same exponent.

Figure 4 shows the calculated extinction from the (C + Ol) mixture of Figure 2 and the contribution to that extinction from the graphite. Graphite is the major contributor to the extinction at all wavelengths. The same is true for the other acceptable mixtures.

According to our models, one or more of the heavy elements (Si, Mg, or Fe) contained in our materials is completely locked up in the grains, naturally into the material used with the graphite. Sometimes, but not always, carbon was also used up. However, lowering the allowed abundance of C relative to H from 3.7×10^{-4} to 2.4×10^{-4} made little difference. but further

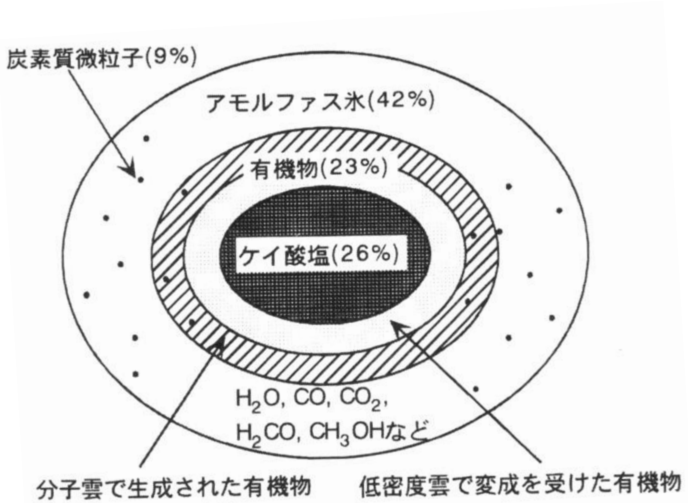

図 7-1　彗星核を構成している固体微粒子[4]。

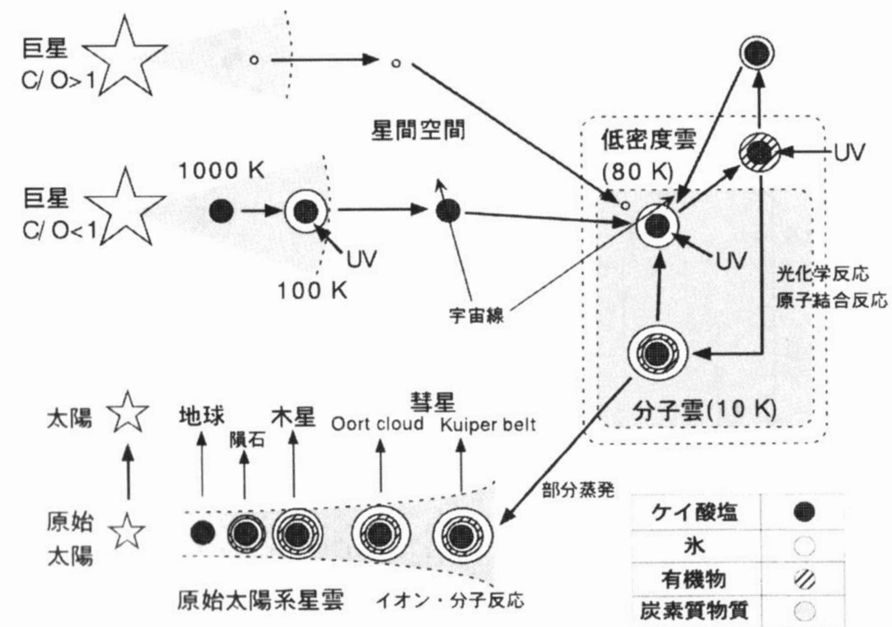

図 7-5　宇宙空間での固体微粒子の一生。

香内晃 2008 宇宙・惑星化学

重力収縮

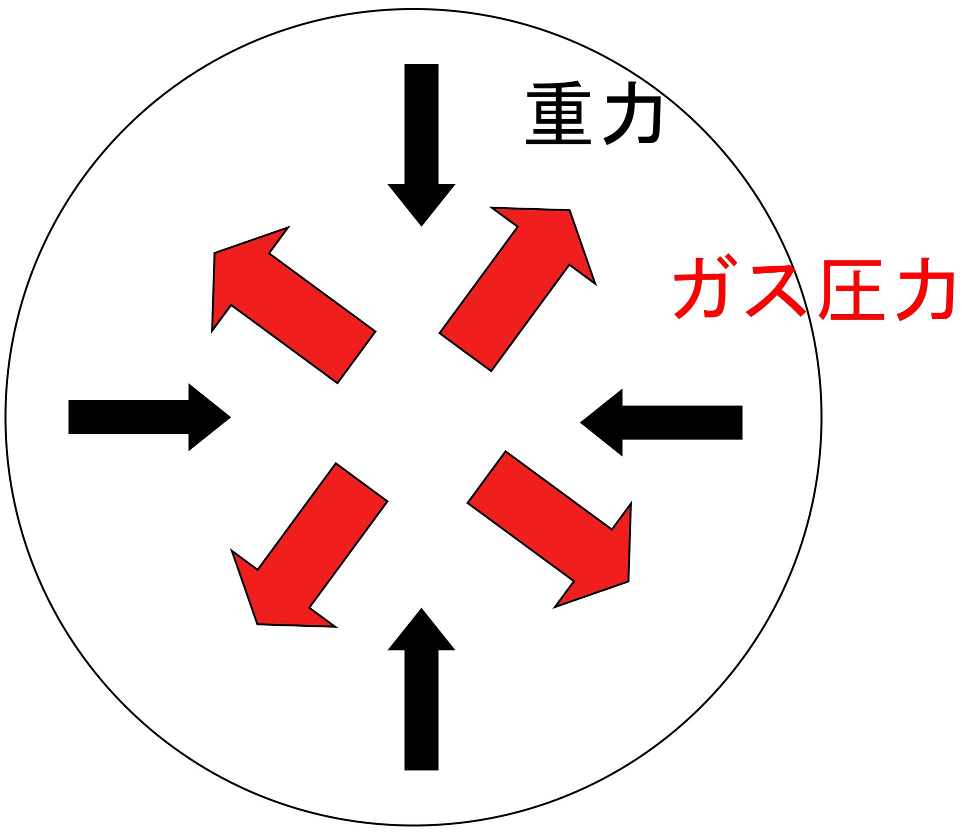

重力不安定

重力 > 圧力

… 重力不安定

重力収縮する

星形成, 分子雲の重力収縮

ガスは冷えないと収縮できない

$$pV = nRT$$

$$dU = nc_V dT = TdS - pdV$$

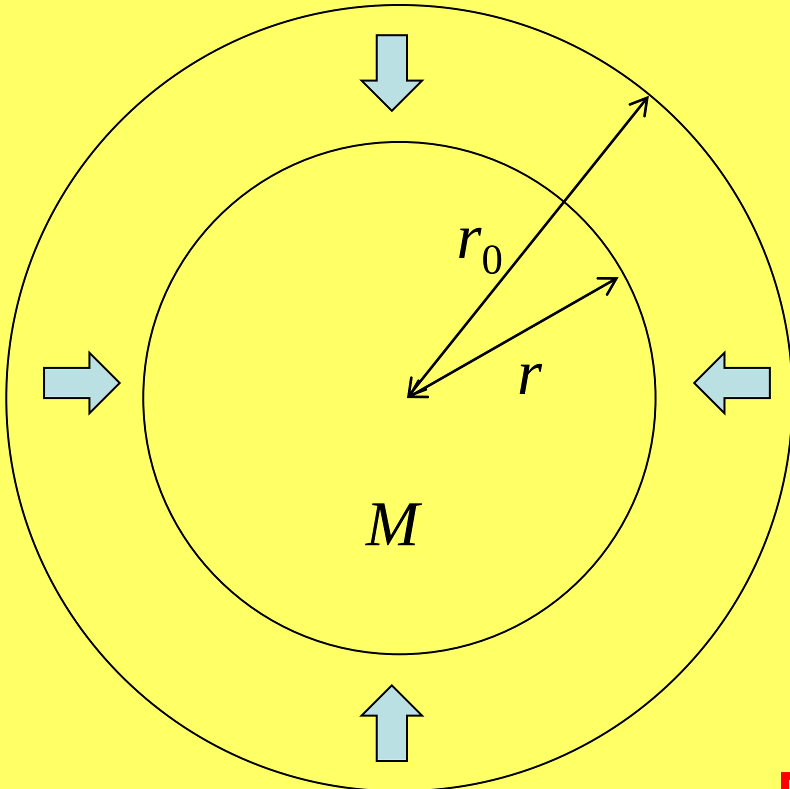

断熱変化のとき

$$pV^{\gamma} = \text{const.} \qquad p = K\rho^{\gamma}$$

$$\left| -\frac{1}{\rho}\frac{dp}{dr} \right| \approx \frac{1}{\rho}\frac{p}{r} \propto r^{-3(\gamma-1)-1}$$

$-3\gamma+2$

$$\left| -\frac{GM}{r^2} \right| \propto r^{-2}$$

$$\boxed{\frac{f_{\mathrm{pres}}}{f_{\mathrm{grav}}} = \left(\frac{f_{\mathrm{pres}}}{f_{\mathrm{grav}}}\right)_0 \left(\frac{r_0}{r}\right)^{3\gamma-4}}$$

Jeans 不安定

温度 = 一定 → c_s = 一定

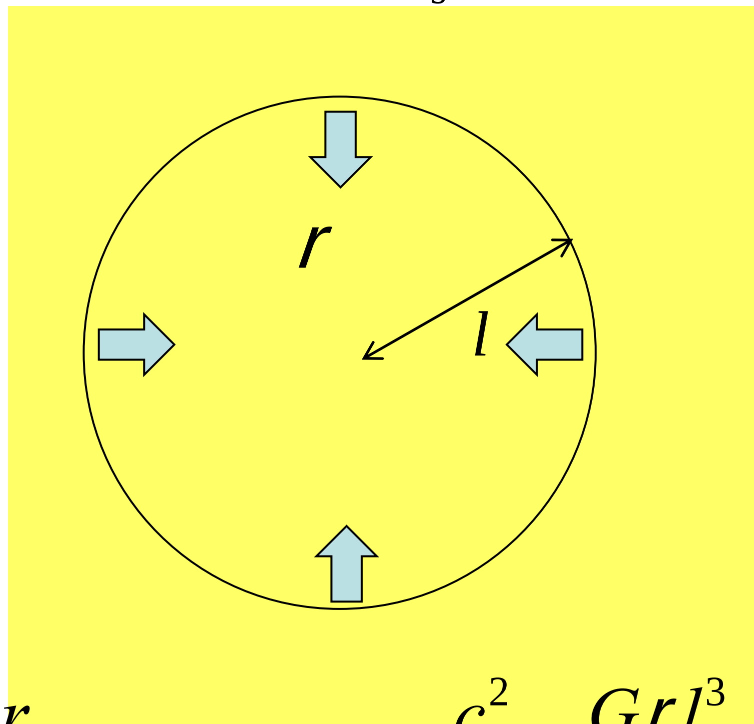

$$p = \frac{\rho}{m} kT = c_s^2 \rho$$

$$f_{\rm pres} = -\frac{1}{\rho}\frac{dp}{dr} \approx \frac{1}{\rho}\frac{p}{\lambda} = \frac{c_s^2}{\lambda}$$

$$f_{\rm grav} = -\frac{G\rho\lambda^3}{\lambda^2}$$

$$\frac{d^2 r}{dt^2} = f_{\rm pres} + f_{\rm grav} = \frac{c_s^2}{\lambda} - \frac{G\rho\lambda^3}{\lambda^2} = \lambda\left(\frac{c_s^2}{\lambda^2} - G\rho\right) \begin{matrix} > \\ < \end{matrix} 0$$

安定
不安定

$$\lambda_J = \frac{c_s}{\sqrt{G\rho}}$$ Jeans 波長

$$M_J = \lambda_J^3 \rho = \left(\frac{c_s}{\sqrt{G\rho}}\right)^3 \rho$$ Jeans 質量

重力不安定（Jeans不安定)

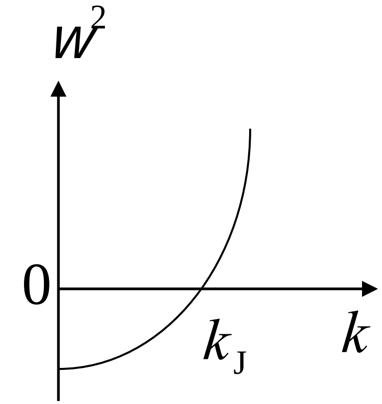

- ガス雲：無限，一様，等方，等温
  磁場，回転無し
- 重力と圧力のみ作用

$$\frac{\partial \rho_1}{\partial t} + \rho_0 \nabla \cdot \mathbf{v}_1 = 0$$

$$\frac{\partial \mathbf{v}_1}{\partial t} = -\frac{c_s^2}{\rho_0} \nabla \rho_1 + \mathbf{g}_1$$

$$\nabla \cdot \mathbf{g}_1 = -4\pi G \rho_1$$

$$\Downarrow$$

$$\omega^2 = c_s^2 k^2 - 4\pi G \rho_0$$

$$\Rightarrow$$

Jeans不安定

Jeans波長

$$\lambda \geq \lambda_\mathrm{J} = \frac{2\pi}{k_\mathrm{J}} = c_s \left(\frac{\pi}{G\rho_0} \right)^{1/2}$$

Jeans質量

$$M \geq M_\mathrm{J} = \frac{4\pi}{3} \rho_0 \left(\frac{\lambda_\mathrm{J}}{2} \right)^3 = \frac{\pi^{5/2}}{6} \frac{c_s^3}{G^{3/2} \rho_0^{1/2}}$$

自由落下時間 (Free Fall Time)

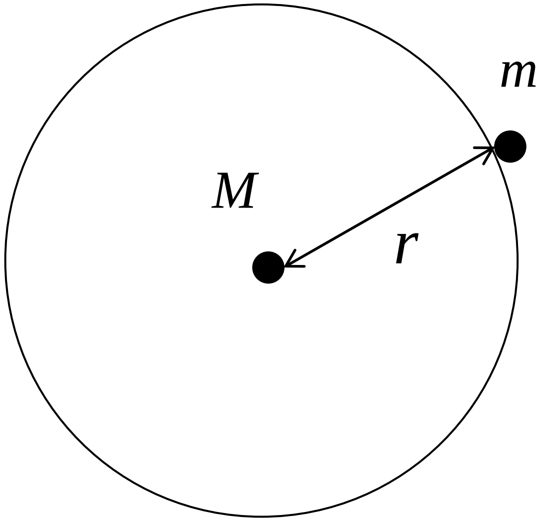

$$\frac{d^2r}{dt^2} = -\frac{GM}{r^2}$$

初期条件: $v = 0$

τ_{ff} : 質点mが原点に達する時間

$$\frac{r}{t_{\mathrm{ff}}^2} = \frac{GM}{r^2} \Rightarrow \boxed{t_{\mathrm{ff}} = \frac{1}{\sqrt{G\rho}}} \quad \rho = \frac{M}{r^3}$$

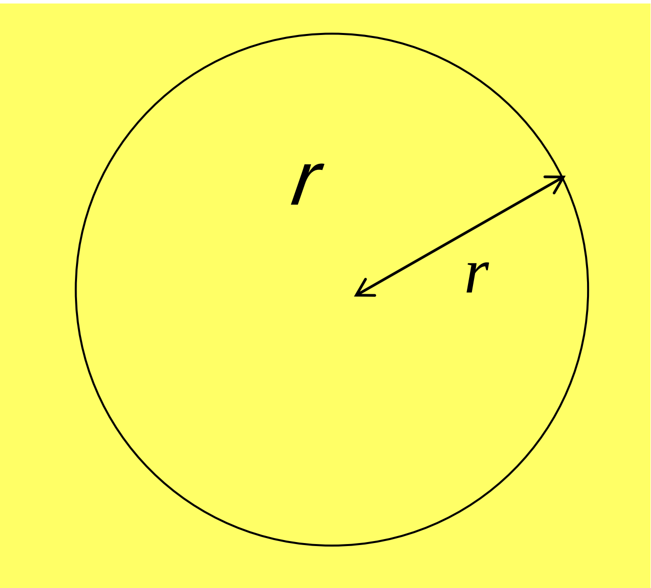

$$\frac{d^2r}{dt^2} = -\frac{GM}{r^2}$$

圧力 $p = 0$
初期条件: $v = 0$

τ : 球の半径が0になる時間

$$\frac{r}{t_{\mathrm{ff}}^2} = \frac{GM}{r^2} \Rightarrow \boxed{t_{\mathrm{ff}} = \frac{1}{\sqrt{G\rho}}}$$

分子雲コアの自由落下時間

$$t_{\mathrm{ff}} = \frac{1}{\sqrt{G\rho}} = 2\times 10^{5} \left(\frac{n}{10^{5}\ \mathrm{cm}^{-3}} \right)^{-1/2}\ \mathrm{yr}$$

質量降着率

$$\dot{M} \approx \frac{M_J}{t_{\mathrm{ff}}} = \frac{\left(c_s t_{\mathrm{ff}}\right)^3 \rho}{t_{\mathrm{ff}}} = \frac{c_s^3}{G} = \frac{1}{G}\left(\frac{kT}{m}\right)^{3/2}$$

$$= 1.6\times 10^{-6} \left(\frac{T}{10\ \mathrm{K}} \right)^{3/2} M_{\mathrm{sun}}/\mathrm{yr}$$

球対称(1D)な重力収縮：時間変化

Larson 1969, *MNRAS* **145**, 271

log 密度

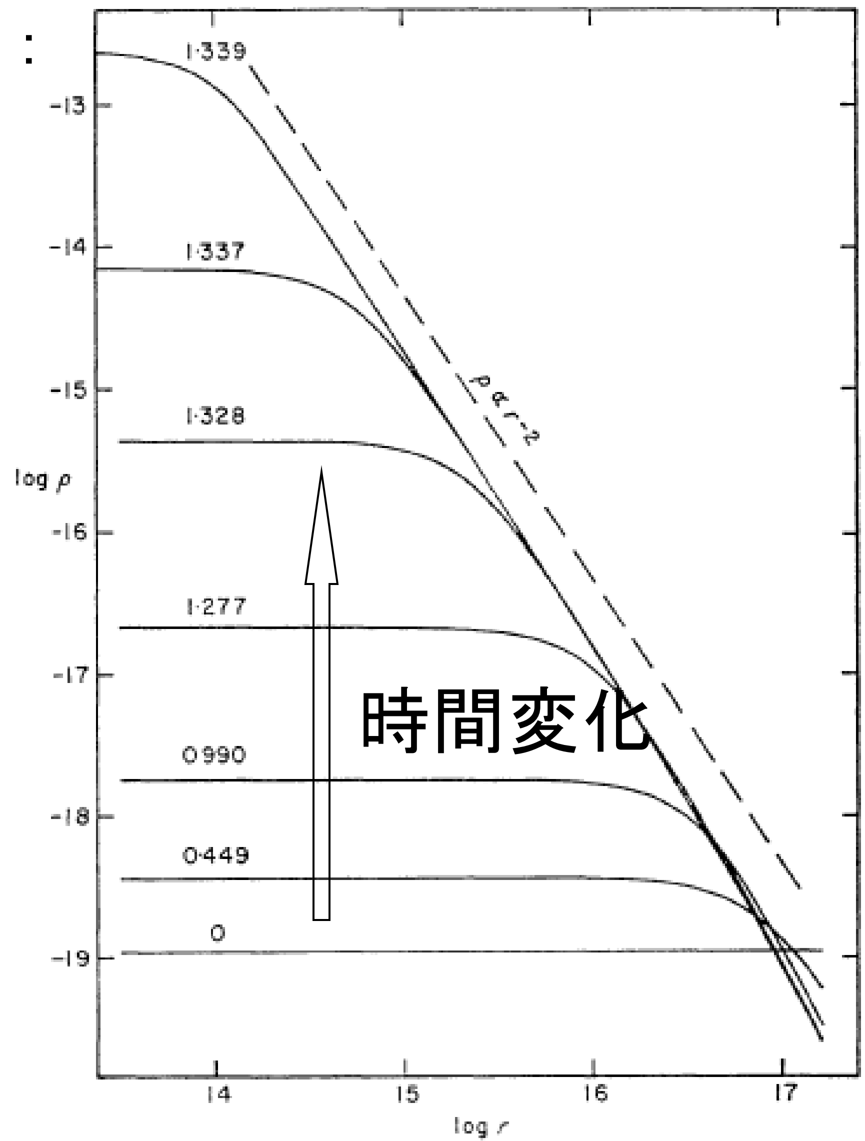

log 距離

参考

$$t = \frac{1}{\sqrt{Gr}}$$

輻射流体力学 基礎方程式系

$$\frac{Dr}{Dt} + r\nabla \cdot \mathbf{v} = 0$$

$$\frac{D\mathbf{v}}{Dt} = -\frac{1}{r}\nabla p + \mathbf{g} + \frac{k}{c}\mathbf{F}$$

$$\frac{D}{Dt}\left(e_{\mathrm{gas}} + \frac{E_{\mathrm{rad}}}{r}\right) + \frac{1}{r}\nabla \cdot \mathbf{F} = \mathrm{G}_{\mathrm{dyn}} + \mathrm{G}_{g} + \mathrm{G}_{\mathrm{CR}}$$

$$\frac{De_{\mathrm{gas}}}{Dt} = \mathrm{G}_{\mathrm{dyn}} + \mathrm{G}_{\mathrm{abs}} - \mathrm{L}_{\mathrm{dust}} + \mathrm{G}_{\mathrm{CR}}$$

$$\frac{D\mathbf{F}}{Dt} = -c^2\nabla \cdot \mathrm{P} - \rho\left(c\kappa + \frac{1}{\rho}\nabla \cdot \mathbf{v}\right)\mathbf{F}$$

$$p = \frac{k_{\mathrm{B}}}{m m_{\mathrm{H}}} r T = (g - 1) r e_{\mathrm{gas}}$$

基本的な流体の式

輻射輸送が関与する式

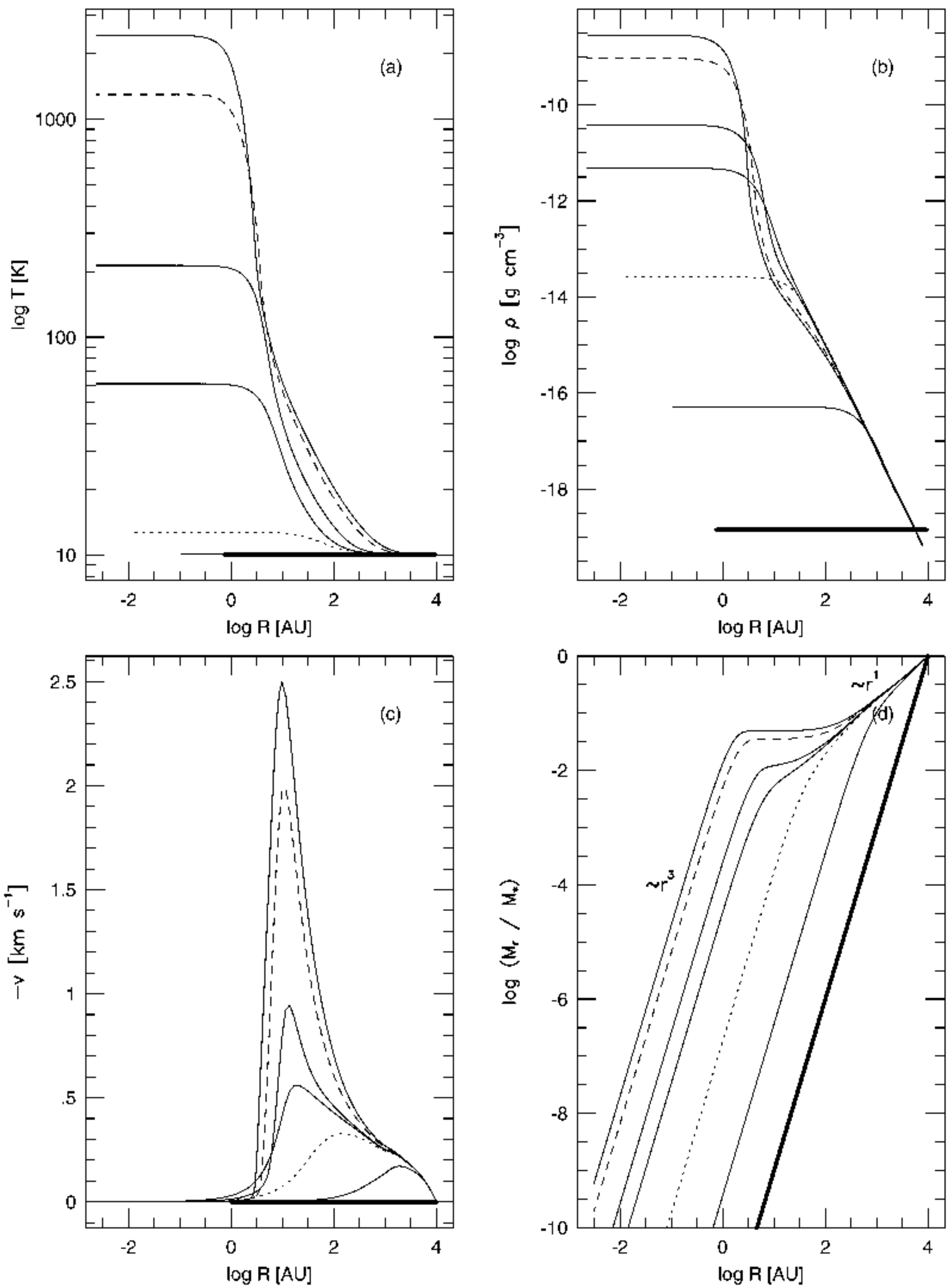

収縮は,
不均質に進行

Masunaga, Miyama,
& Inutsuka 1998

フィラメント状分子雲の収縮と分裂

Ogochi, Nakamoto (in prep.)

初期フィラメント状分子雲

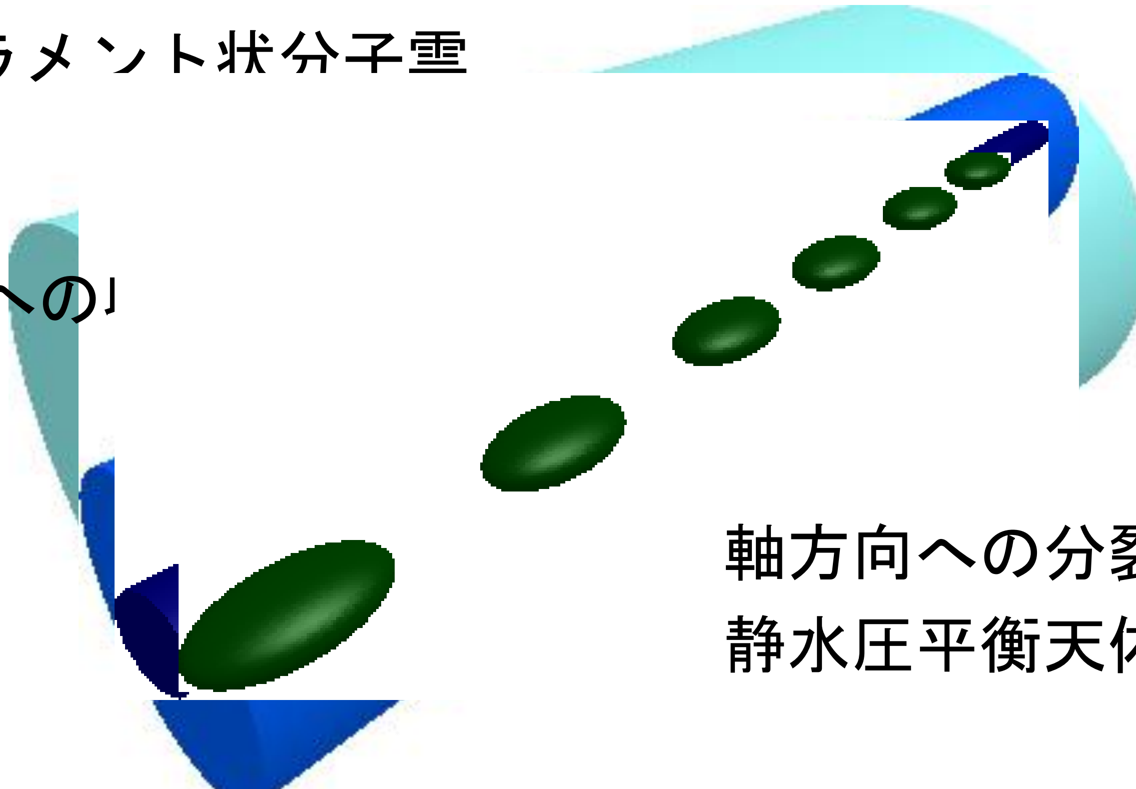

動径方向への

軸方向への分裂：
静水圧平衡天体の形成

動径方向への収縮の停止：状態方程式の変化

中心密度・温度の進化

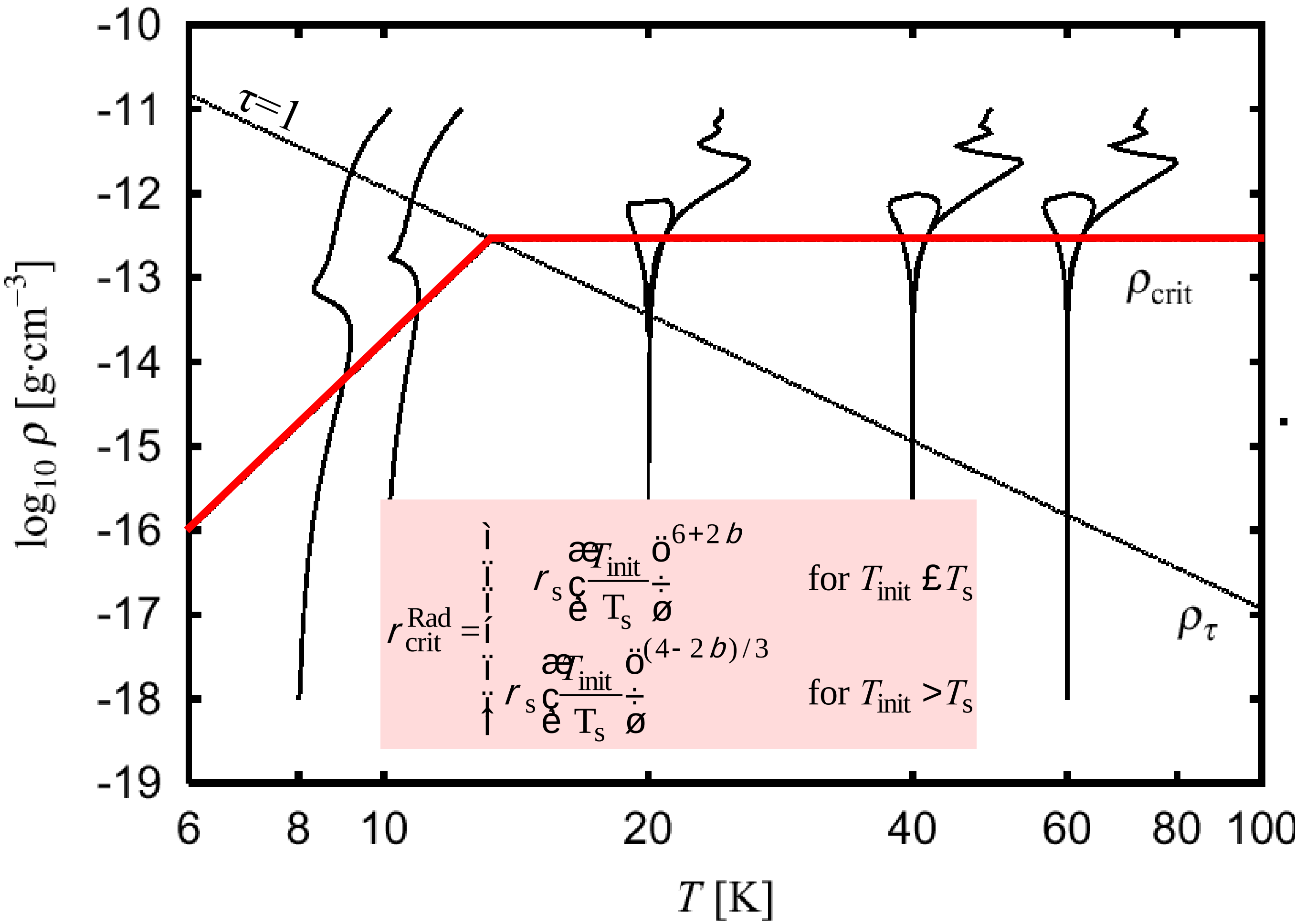

$$\rho_{\rm crit}^{\rm Rad} = \begin{cases} \rho_{\rm s}\left(\dfrac{T_{\rm init}}{T_{\rm s}}\right)^{6+2\beta} & \text{for } T_{\rm init} \le T_{\rm s} \\ \rho_{\rm s}\left(\dfrac{T_{\rm init}}{T_{\rm s}}\right)^{(4-2\beta)/3} & \text{for } T_{\rm init} > T_{\rm s} \end{cases}$$

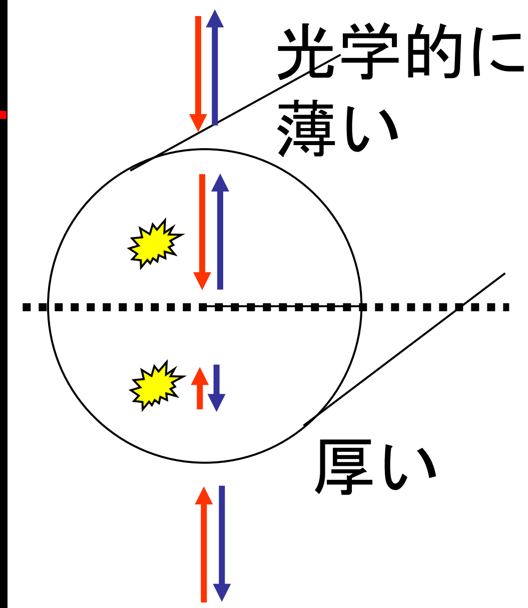

$$\frac{De_{\rm gas}}{Dt} = \Gamma_{\rm dyn} - \Lambda_{\rm dust} + \Gamma_{\rm rad}$$

断熱圧縮加熱

輻射加熱

輻射冷却

Goodman et al. 1993

分子雲コアの
回転を観測

$$\omega = (1-10) \times 10^{-14}\ \mathrm{rad\ s^{-1}}$$

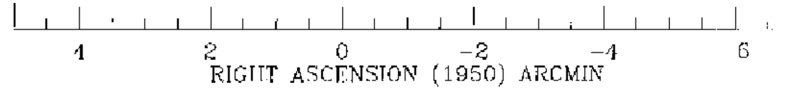

FIG. 3c

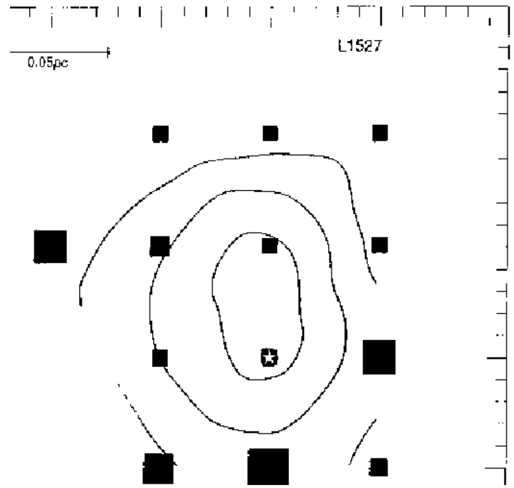

for L1495 are presented in Tables 1 and 2
together, and for each of the two clumps sep
Fitting a complex of clumps together of
ferent result than fitting pieces individually
show that combinations of the gradients
clumps labeled "L1495SE" and "L1495N
and "B217SW," clearly do not suggest
to all of L1495, or B217, respectively. Th
just observing smaller pieces of a coheren
gradient.
The mean LSR velocity of L1495SE diffe
L1495NW by 0.6 km s^{-1}, more than twice
The velocity map in Figure 4*a* makes it p
clumps are kinematically distinct. Therefor
data for the "whole cloud," we are actu
motion of one clump with respect to ano
smooth gradient over the whole map. It is
of lower density tracers (such as $C^{18}O$), m

534 GOODM

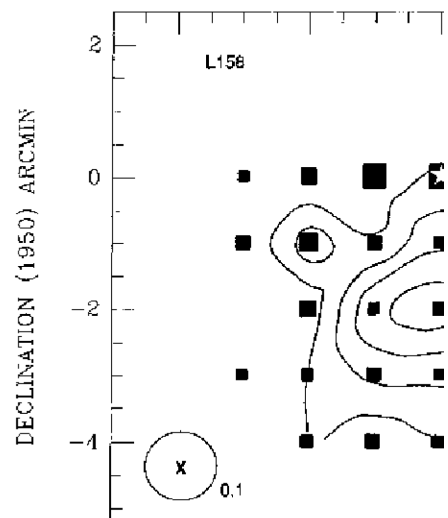

IRAM 04191

Belloche et al. 2002

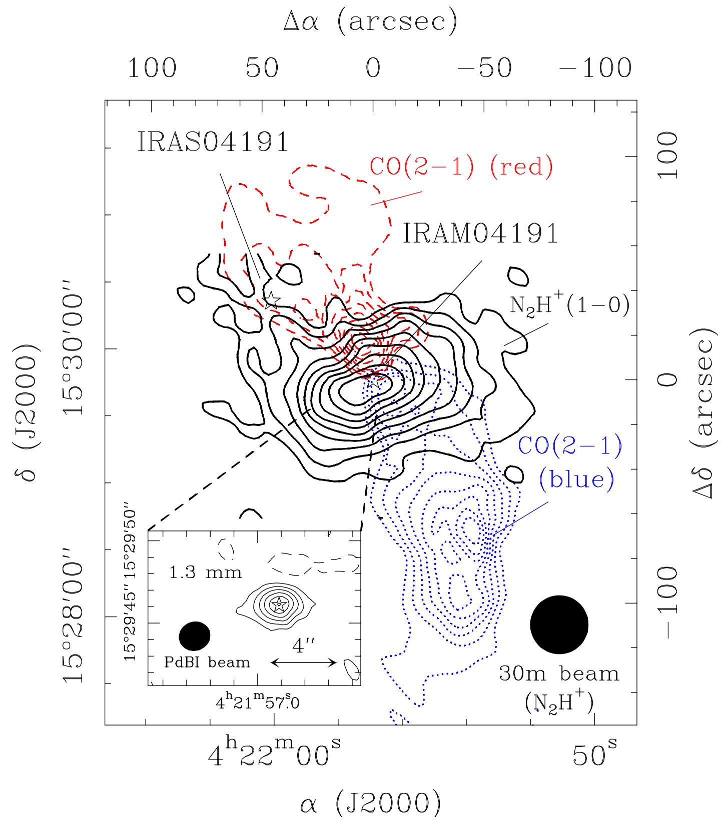

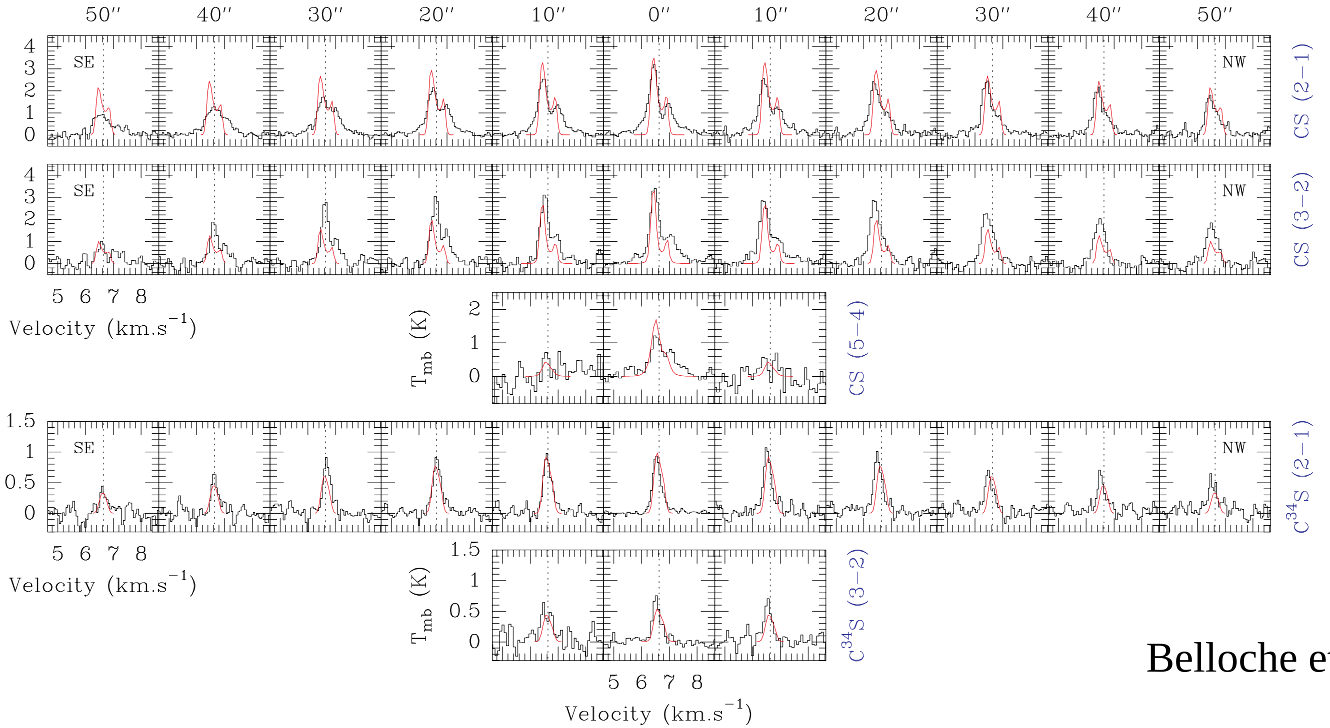

Fig. 8. CS(2–1), CS(3–2), CS(5–4), $C^{34}S$(2–1), and $C^{34}S$(3–2) spectra (in units of main beam temperature) observed along the direction perpendicular to the outflow axis (histograms). The dotted line indicates our best-fit estimate (6.63 km s^{-1}) of the envelope systemic velocity based on our CS/$C^{34}S$ modeling. Synthetic spectra corresponding to the "best-fit" 1D spherical collapse model described in Sect. 4.3 (cf. Figs. 7 and 12a,b for model parameters) are superimposed.

Belloche et al. 2002

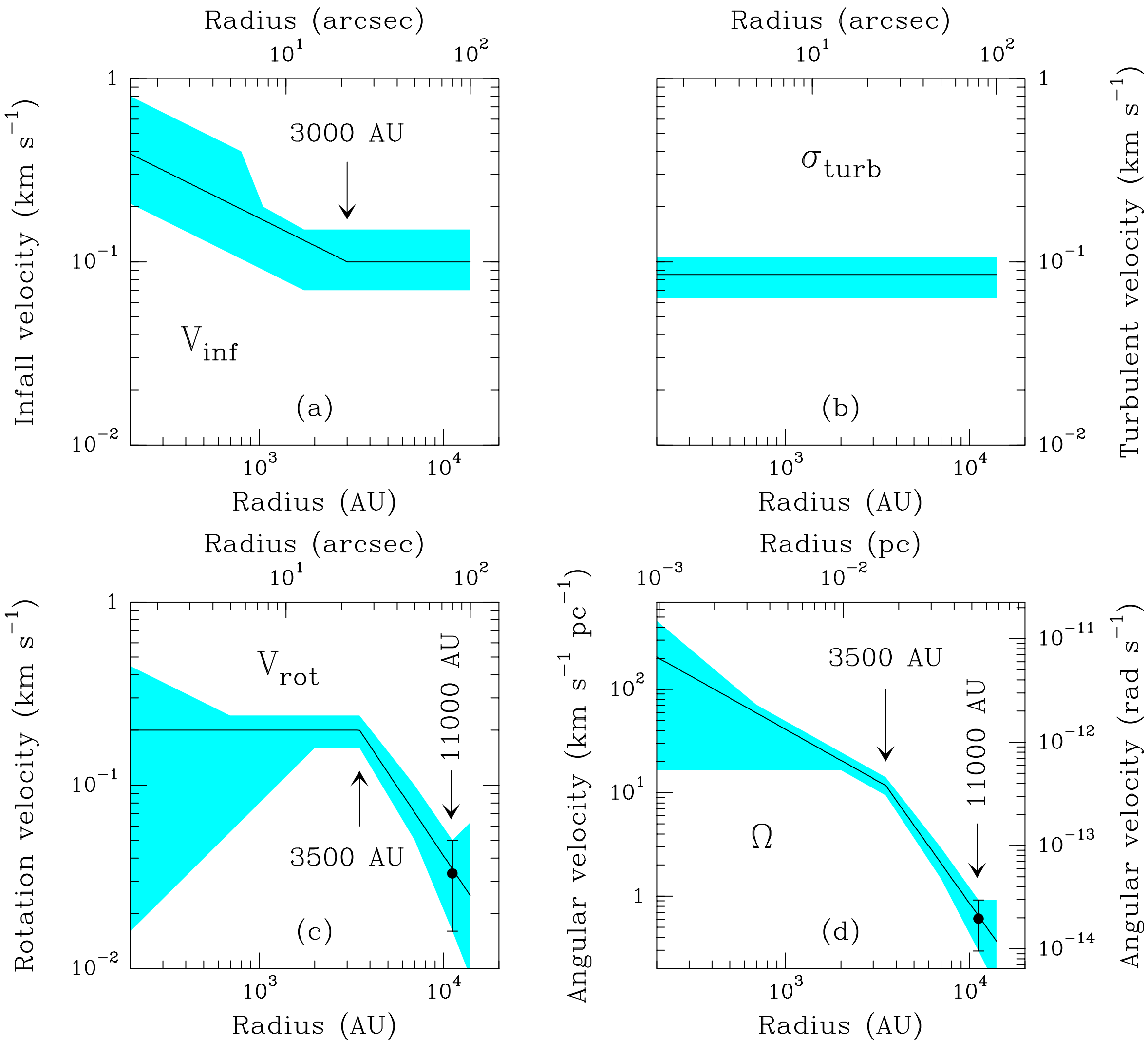

Fig. 12. Infall a), turbulence b), and rotation c) velocity fields inferred in the IRAM 04191 envelope based on our 1D (Sect. 4) and 2D (Sect. 5) radiative transfer modeling. The shaded areas show the estimated domains where the models match the CS and $C^{34}S$ observations reasonably well. In a) and b), the solid lines show the infall velocity and turbulent velocity dispersion in both the 1D and 2D models (cf. Figs. 8 and 14, respectively) as a function of radius from envelope center. In c), the solid line represents the profile of the azimuthal rotation velocity in the 2D envelope model (cf. Fig. 14) as a function of radius from the outflow/rotation axis. The point with error bar at 11 000 AU corresponds to the velocity gradient observed in $C^{18}O$ (cf. Sect. 3.2). Panel d) shows the corresponding angular velocity profile.

Belloche et al. 2002

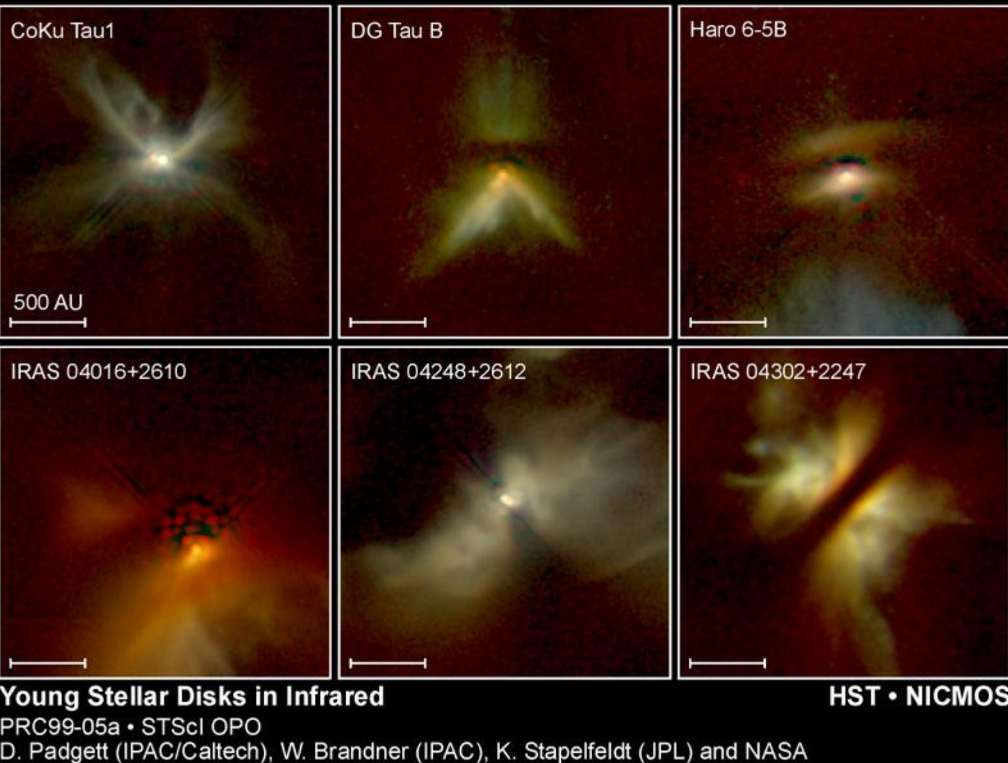

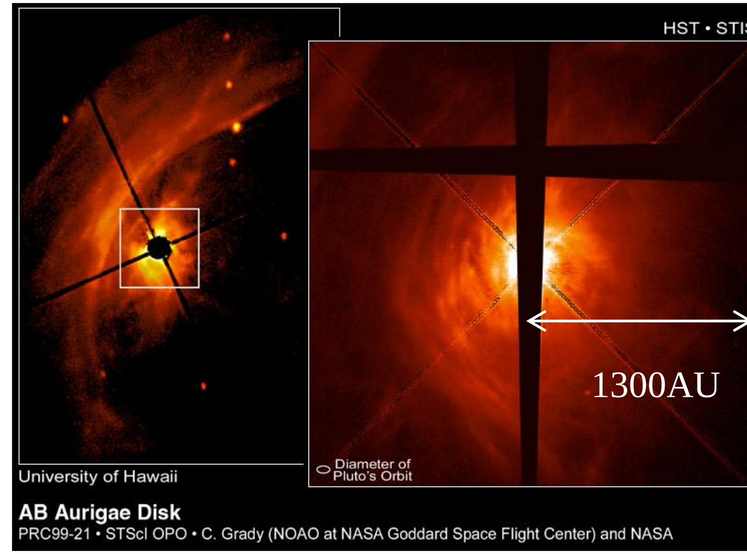

アウトフロ
（双極分子

原始惑星系

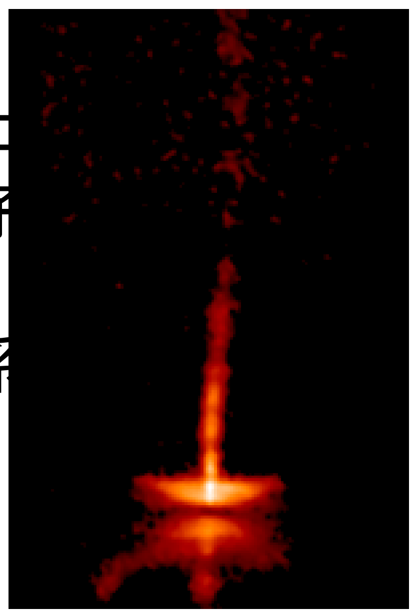

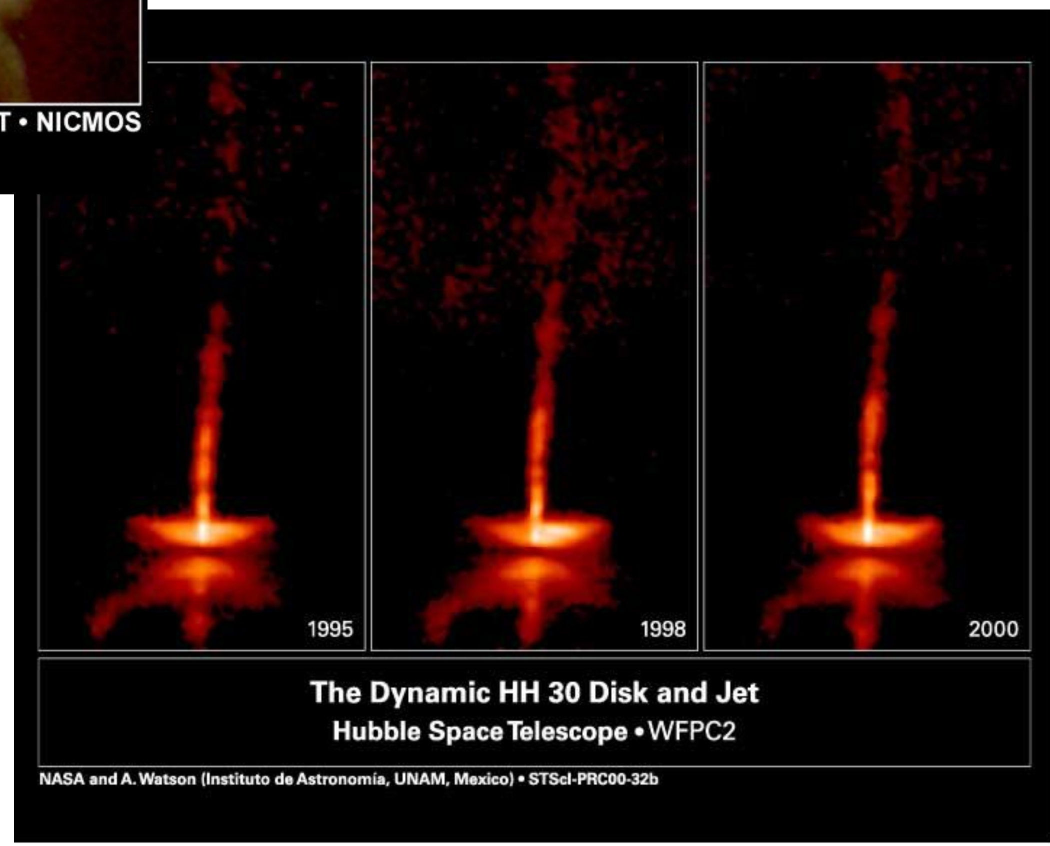

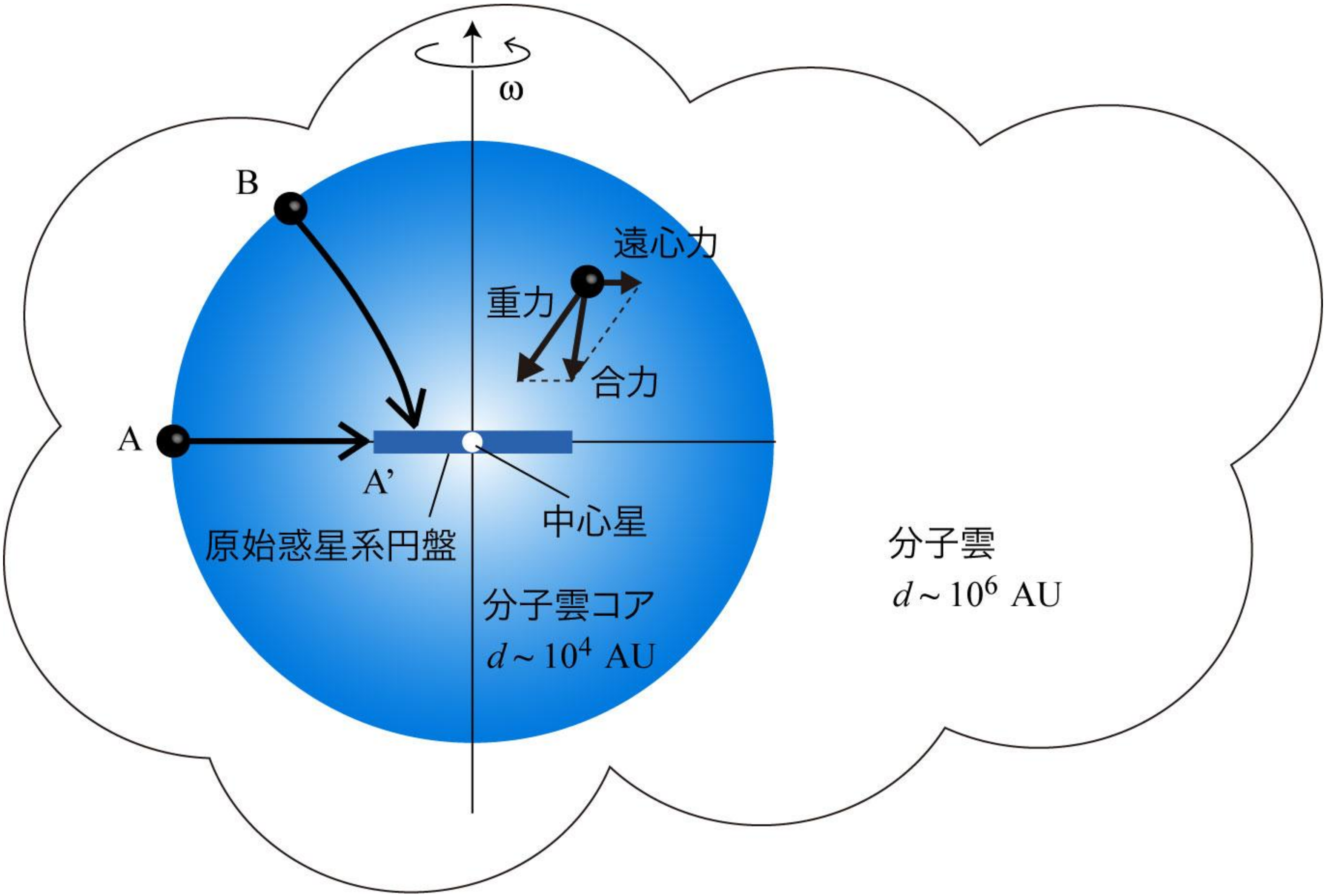
ω
B
遠心力
重力
合力
A
A'
中心星
原始惑星系円盤
分子雲コア
d ~ 10^4 AU
分子雲
d ~ 10^6 AU

分子雲コアの重力収縮の数値シミュレーション

松本倫明氏（法政大学）

・3D自己重力流体計算
・Nested Grid法

回転している分子雲コアの収縮
円盤・バー構造の形成

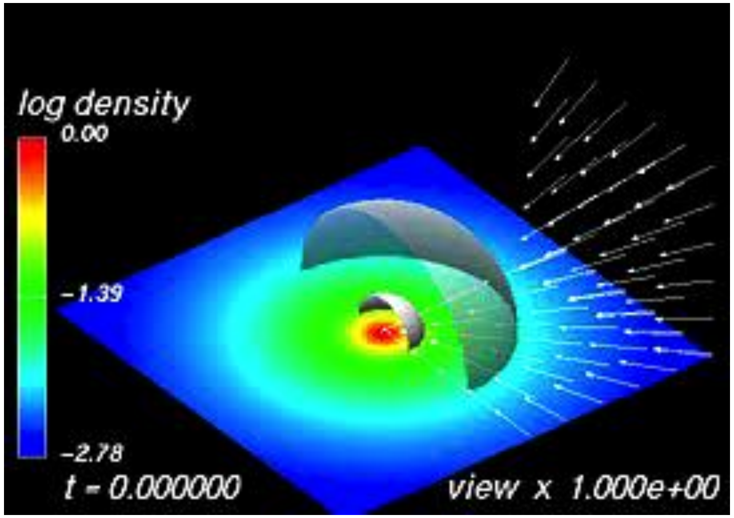

星コアの形成

密度分布

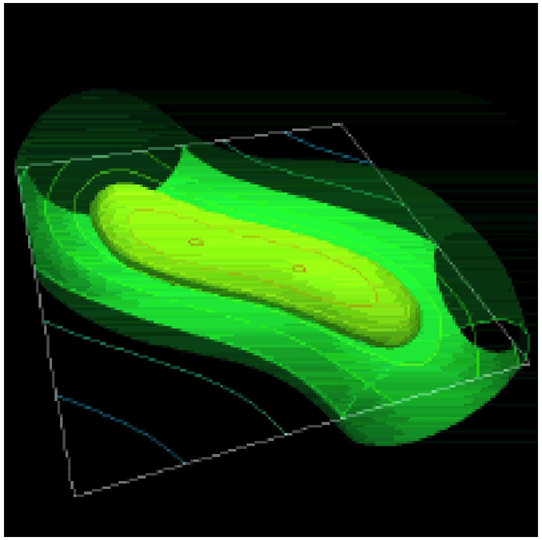

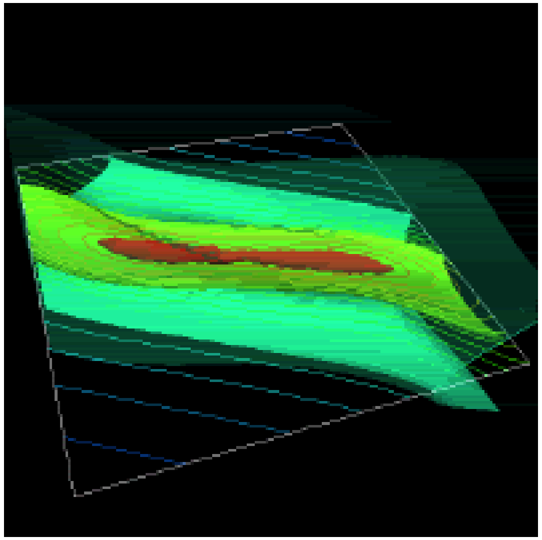

1/2細かい格子

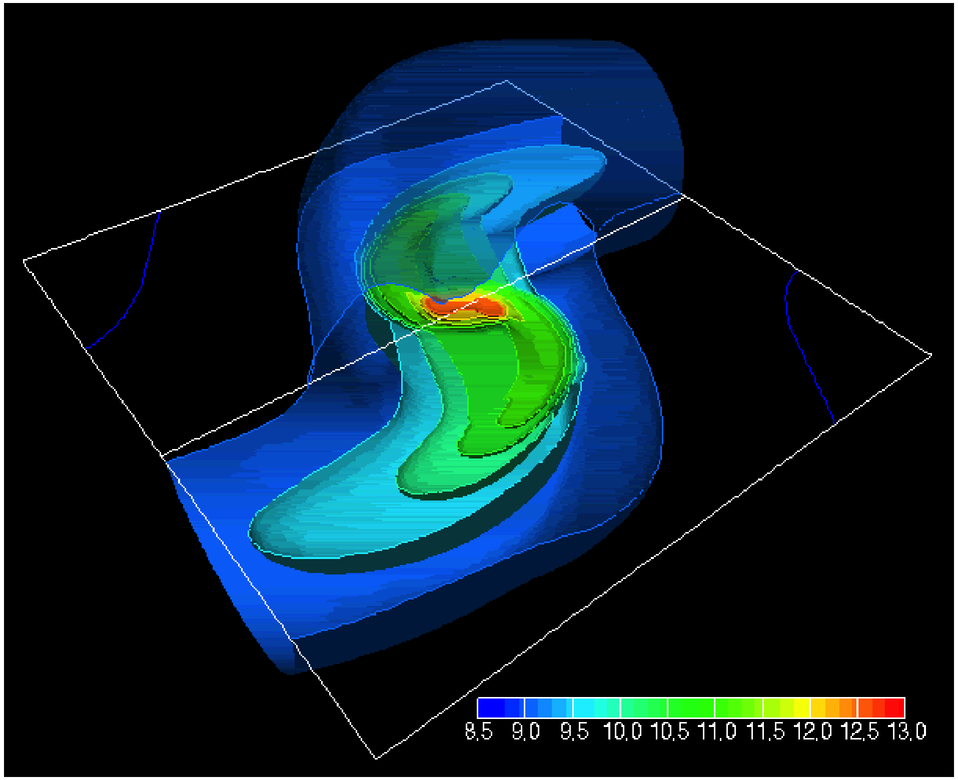
8.5 9.0 9.5 10.0 10.5 11.0 11.5 12.0 12.5 13.0

連星系の形成

Matsumoto & Hanawa 2003

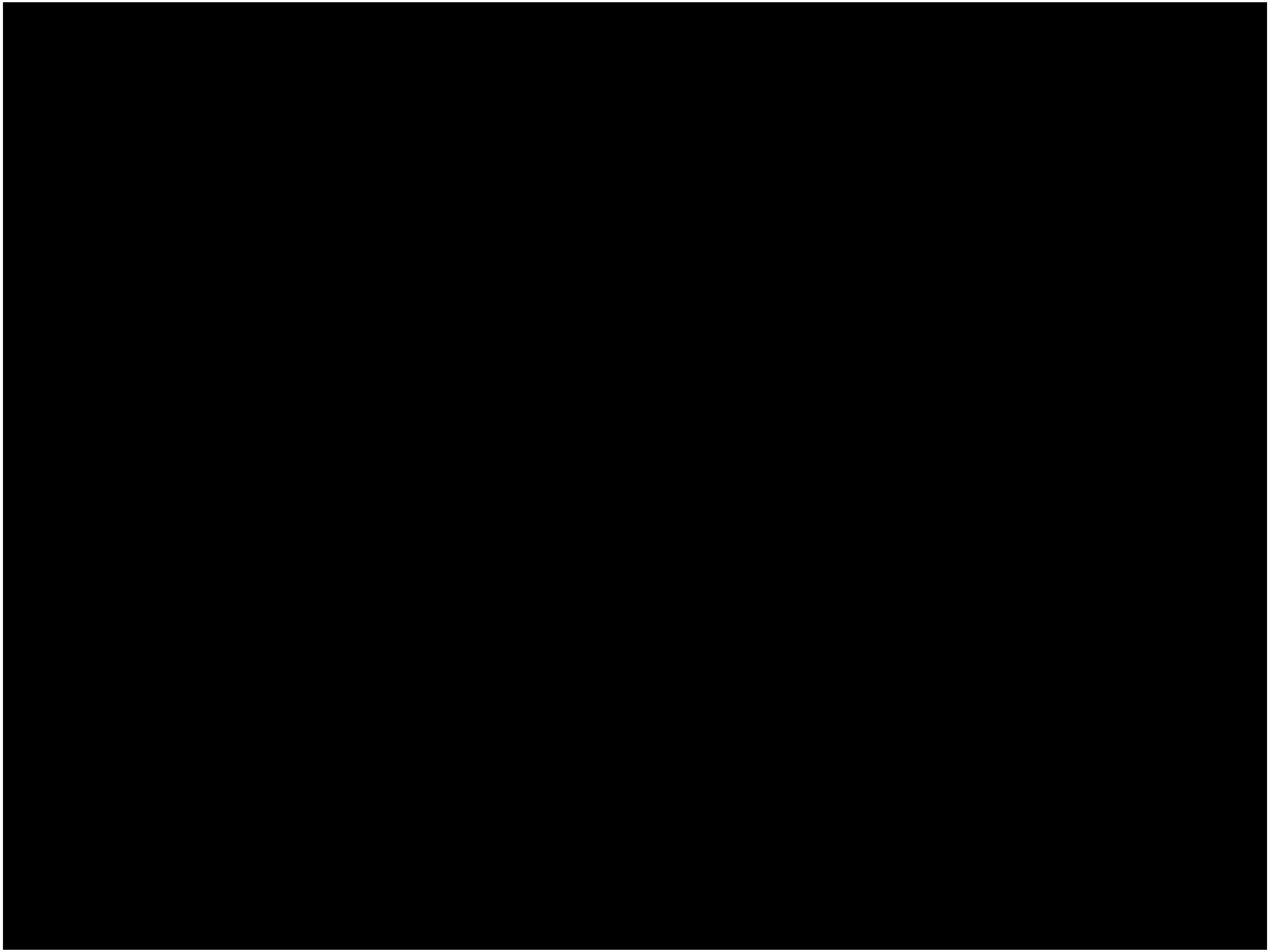

国立天文台４次元デジタル宇宙プロジェクト提供

磁場の効果，ジェットの形成

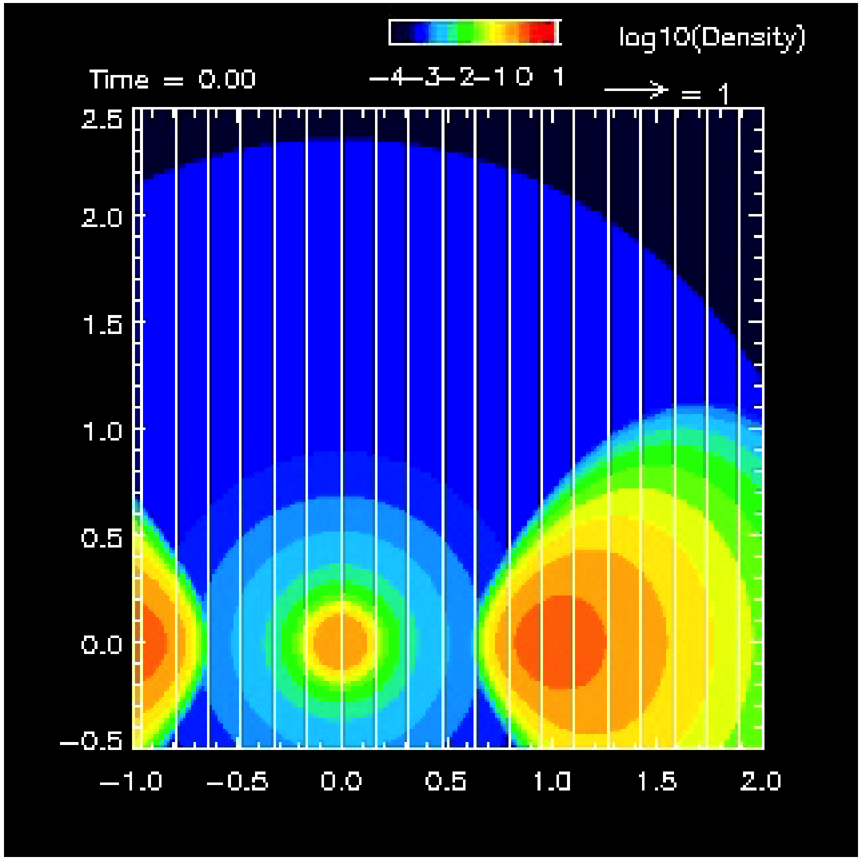

工藤哲洋氏（国立天文台）

アウトフローの生成

Matsumoto & Tomisaka 2004

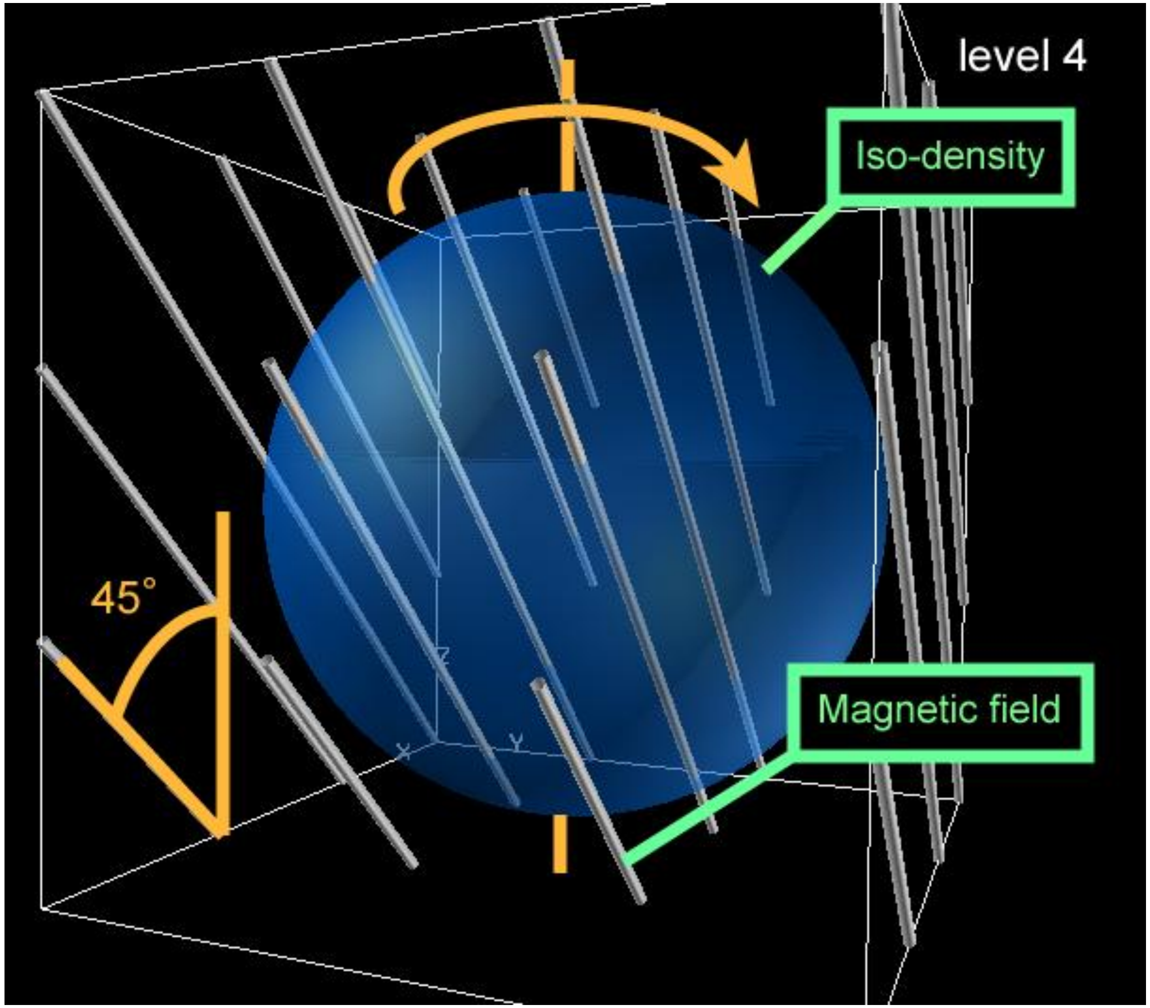

松本倫明氏(法政大学)

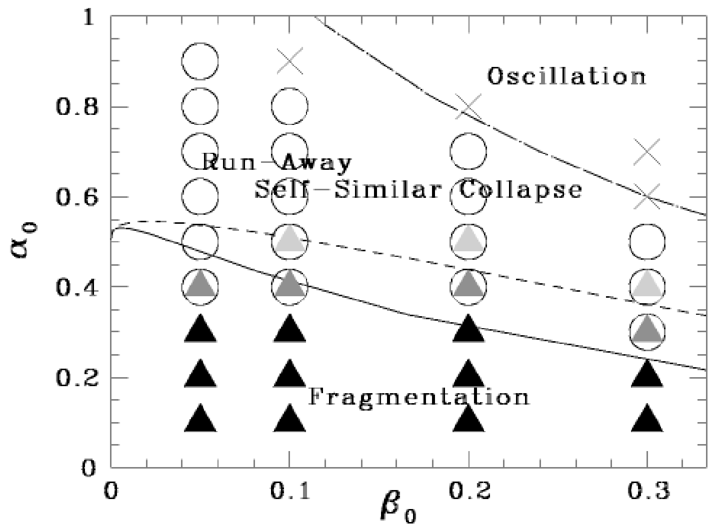

FIG. 3.—Criteria for collapse and fragmentation of the rotating isothermal clouds. Results for the initial ring-mode and bar-mode perturbation for various initial amplitudes are plotted. Crosses, circles, and triangles represent the oscillation, collapse without fragmentation, and fragmentation, respectively, in the three-dimensional numerical calculations. The gray scale for triangles corresponds to the initial amplitude. Black, dark gray, and light gray represent $\delta_\rho \sim 0.05$, 0.15, and 0.5, respectively. Some of the results depend on the amplitude of initial perturbations (e.g., in the case of $\alpha = 0.4$ and $\beta = 0.1$, the cloud fragments for $\delta_\rho \sim 0.15$ and collapses without fragmentation for $\delta_\rho \sim 0.05$). The solid line represents the condition that the central flatness is 4π at the epoch of the centrifugal bounce, below which fragmentation is expected. The dashed line represents the condition that the rarefaction wave in the cylindrical radial direction reaches the center at the centrifugal bounce epoch, above which the cloud is expected to approaches to the runaway collapsing self-similar solution. These criteria are derived semianalytically by Tsuribe & Inutsuka (1999a). The dash-dotted line is the criterion for collapse derived by Kiguchi et al. (1987).

Tsuribe & Inutsuka 1999

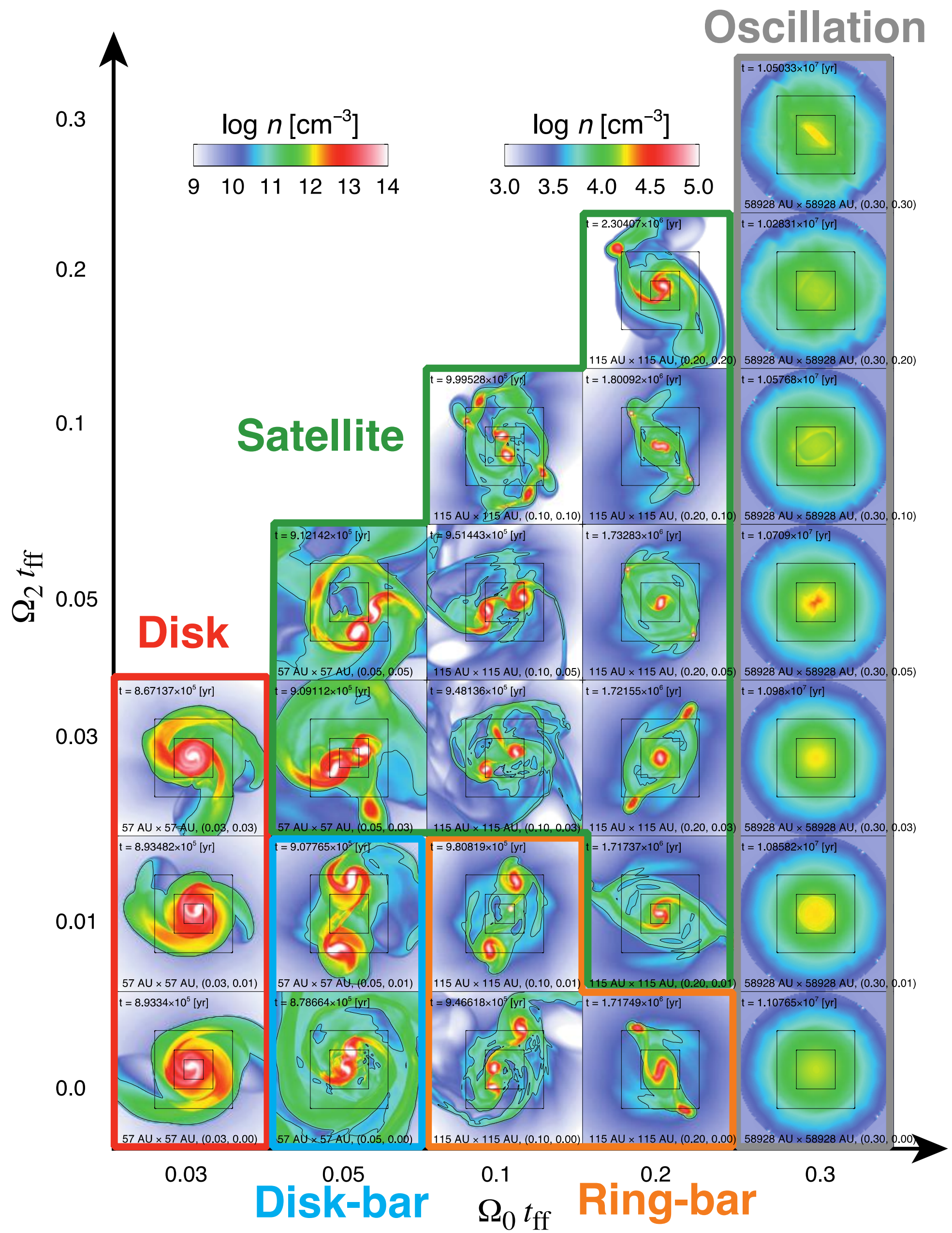

Matsumoto & Hanawa 2003

FIG. 2.—Density distributions in the $z = 0$ plane at the last stages for models for which $C = 0$. Color denotes the density distribution on a logarithmic scale. The right color scale is for *oscillation* models, and the left color scale is for models of disk, satellite, ring-bar, and disk-bar types. Black contour curves denote the critical density n_{cr}. Panels are arranged in the order $\Omega_0 t_{ff} = 0.03$, 0.05, 0.1, 0.2, and 0.3 from left to right, and $\Omega_2 t_{ff} = 0.0$, 0.01, 0.03, 0.05, 0.1, 0.2, and 0.3 from bottom to top.

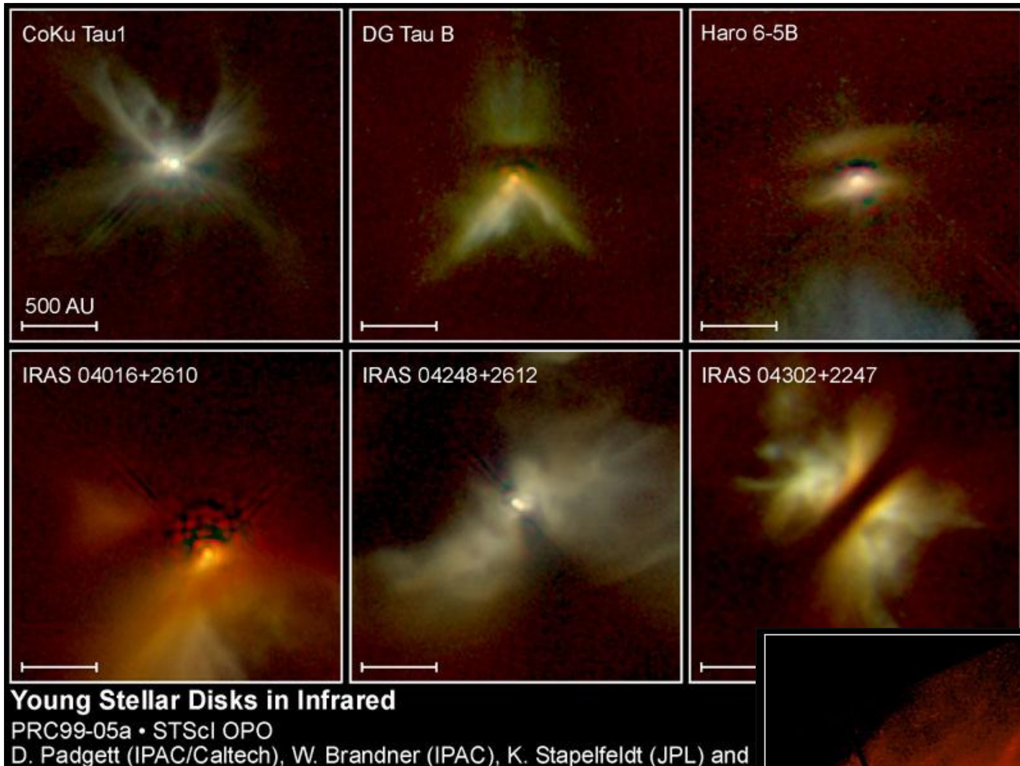
CoKu Tau1
DG Tau B
Haro 6-5B
500 AU
IRAS 04016+2610
IRAS 04248+2612
IRAS 04302+2247
Young Stellar Disks in Infrared
PRC99-05a • STScI OPO
D. Padgett (IPAC/Caltech), W. Brandner (IPAC), K. Stapelfeldt (JPL) and

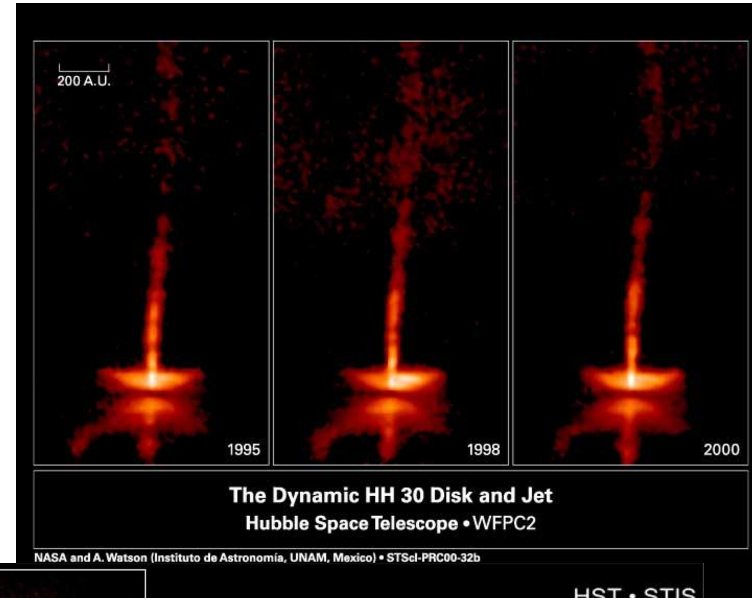
200 A.U.
1995
1998
2000
The Dynamic HH 30 Disk and Jet
Hubble Space Telescope • WFPC2
NASA and A. Watson (Instituto de Astronomía, UNAM, Mexico) • STScI-PRC00-32b

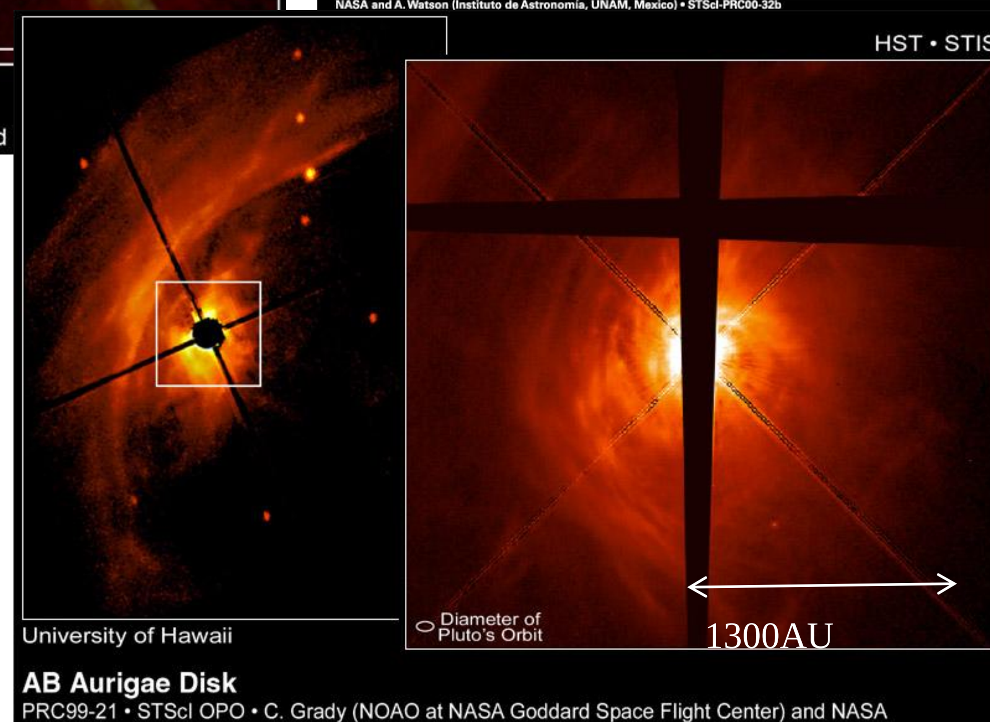
HST • STIS
University of Hawaii
Diameter of Pluto's Orbit
1300AU
AB Aurigae Disk
PRC99-21 • STScI OPO • C. Grady (NOAO at NASA Goddard Space Flight Center) and NASA

原始惑星系円盤

原始惑星系円盤の形成

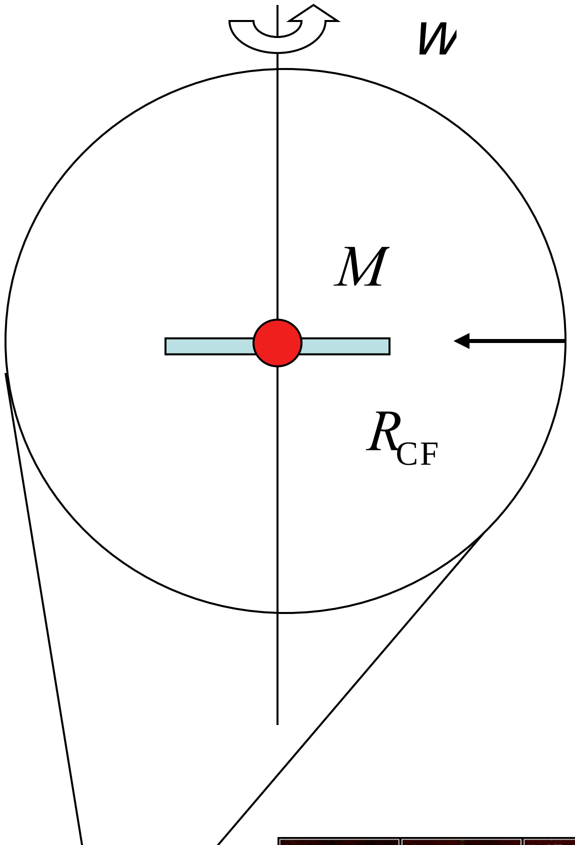

角運動量

$$j = r^2 \omega$$

重力 = 遠心力

$$\frac{GM}{R_{CF}^2} = \frac{j^2}{R_{CF}^3}$$

$$R_{CF} = \frac{j^2}{GM} = \frac{r^4 \omega^2}{GM}$$

$$R_{CF} = 25 \left(\frac{r}{10^4 AU} \right)^4 \left(\frac{\omega}{10^{-14} s^{-1}} \right)^2 \left(\frac{M}{M_{sun}} \right)^{-1} \mathrm{AU}$$

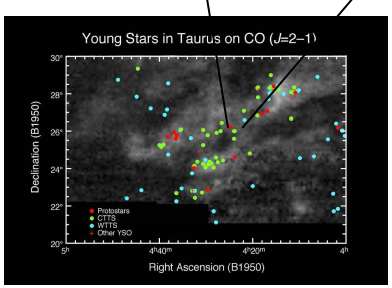

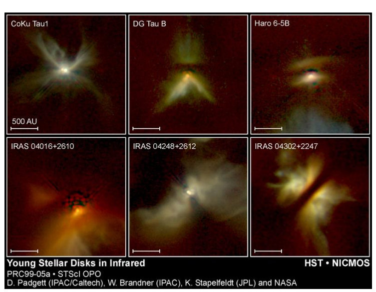

星+円盤系の形成

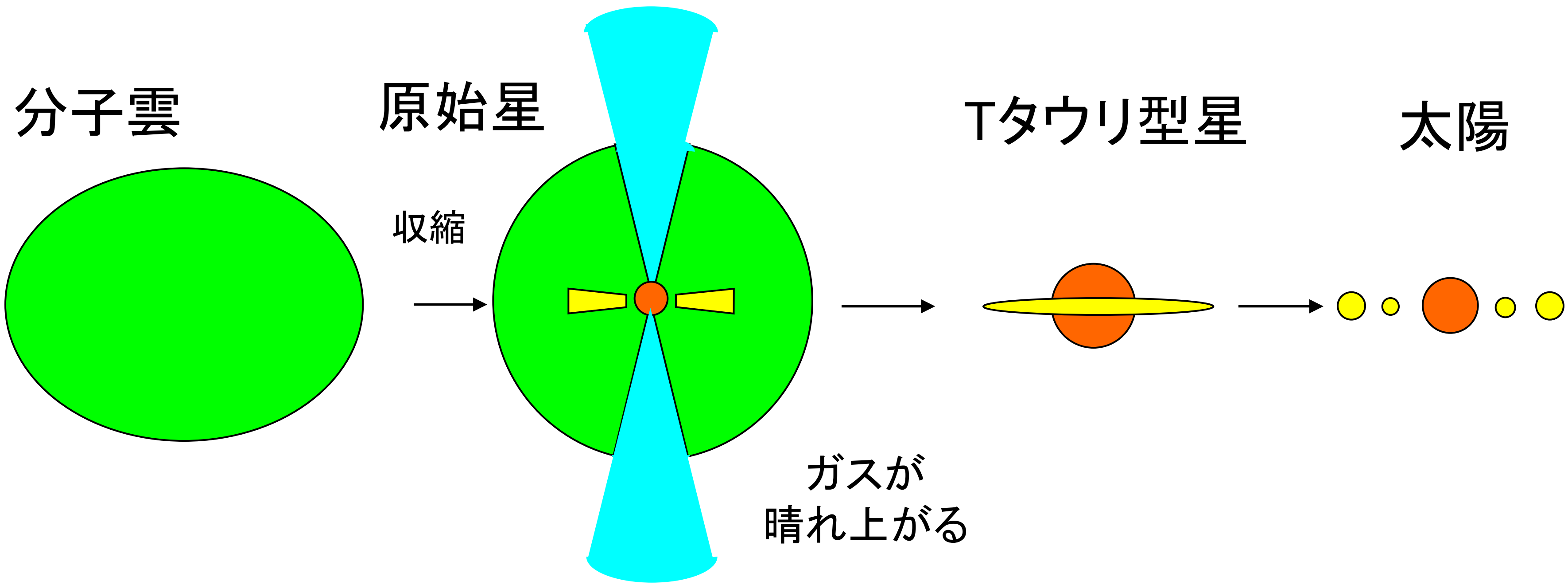

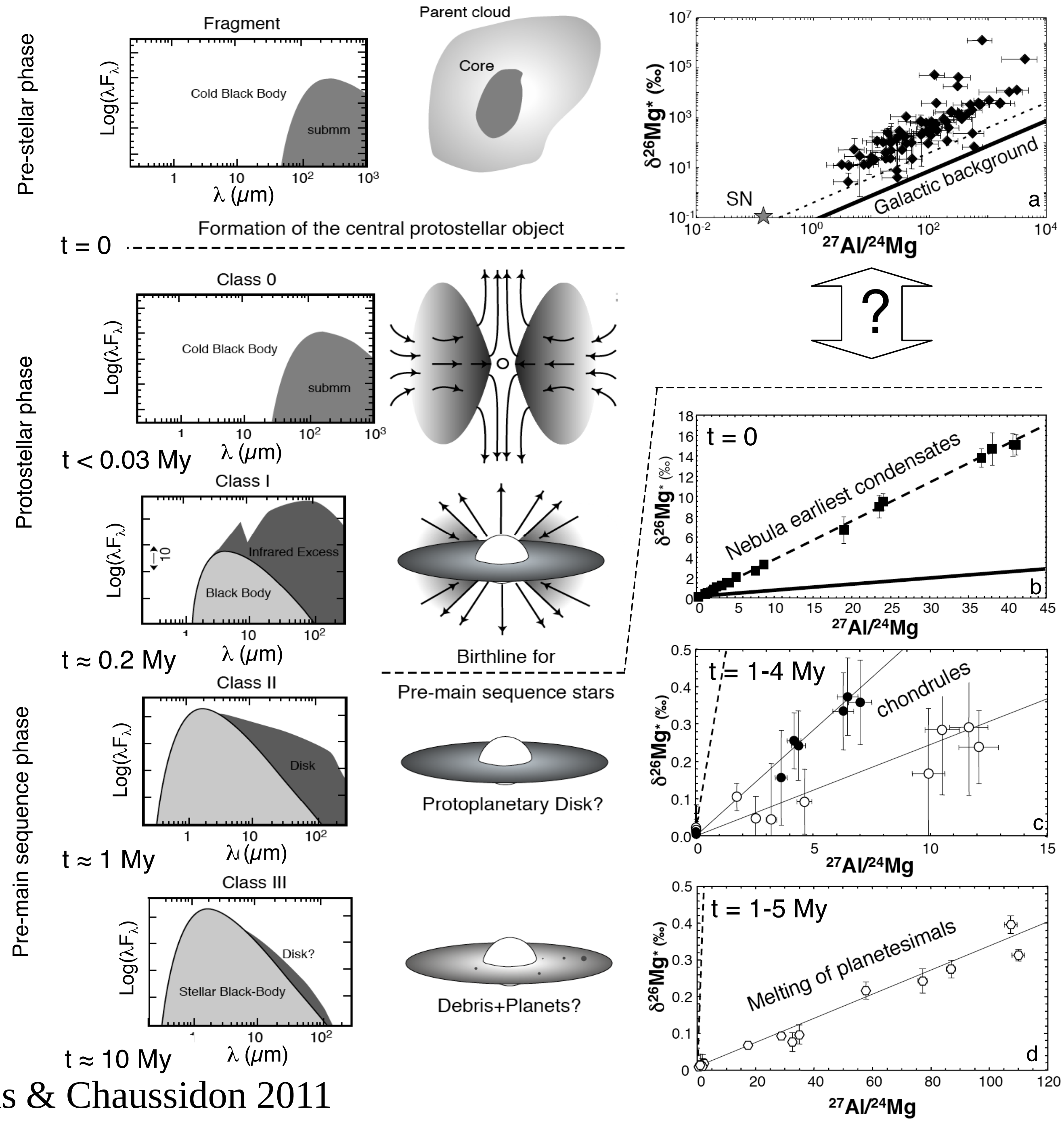

Dauphas & Chaussidon 2011

モデル

- 2次元軸対称
- 4成分;
  中心コア、星周円盤、
  エンベロープ、双極分子流
- モデルを特徴付ける物理量

中心コア; 光度 L_{star}
星周円盤; 面密度分布

$$\Sigma(r) = \Sigma_1 \left(\frac{r}{1\mathrm{AU}} \right)^{-q}$$

エンベロープ; 密度分布

$$\rho(r) = \rho_1 \left(\frac{r}{1\mathrm{AU}} \right)^{-p}$$

bipolar outflow; opening angle θ_{bp}
観測角度; i

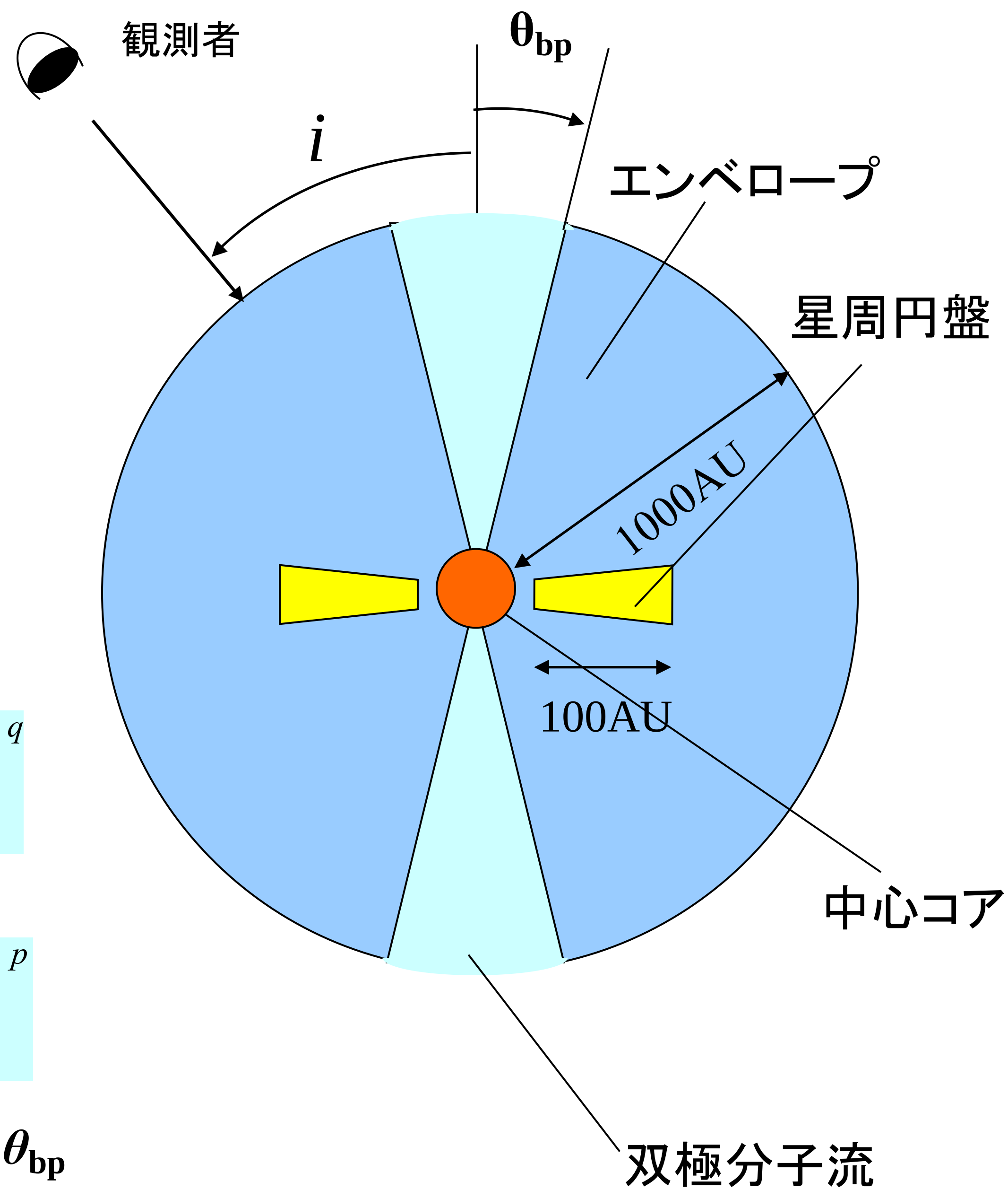

原始星

Nakazato, Nakamoto, & Kikuchi 2003

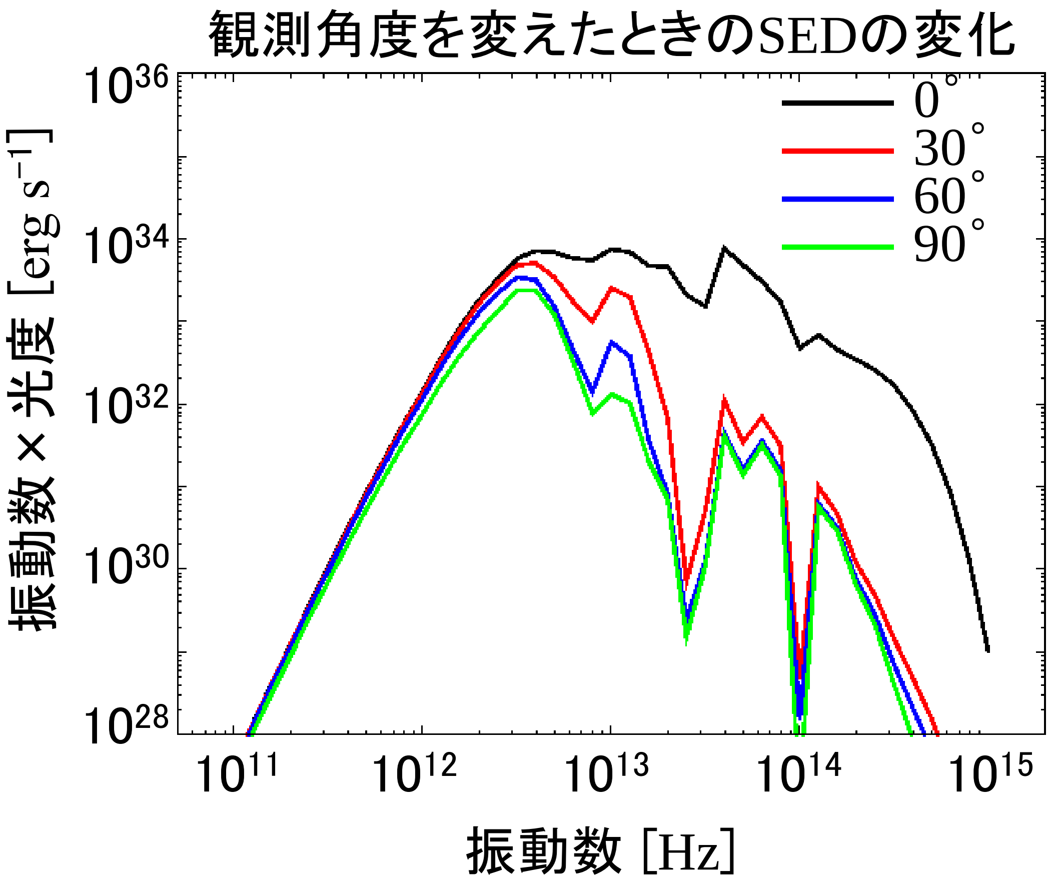

Tタウリ型星のスペクトル

Beckwith *et al*. 1990, AJ **99**, 924

フラックス

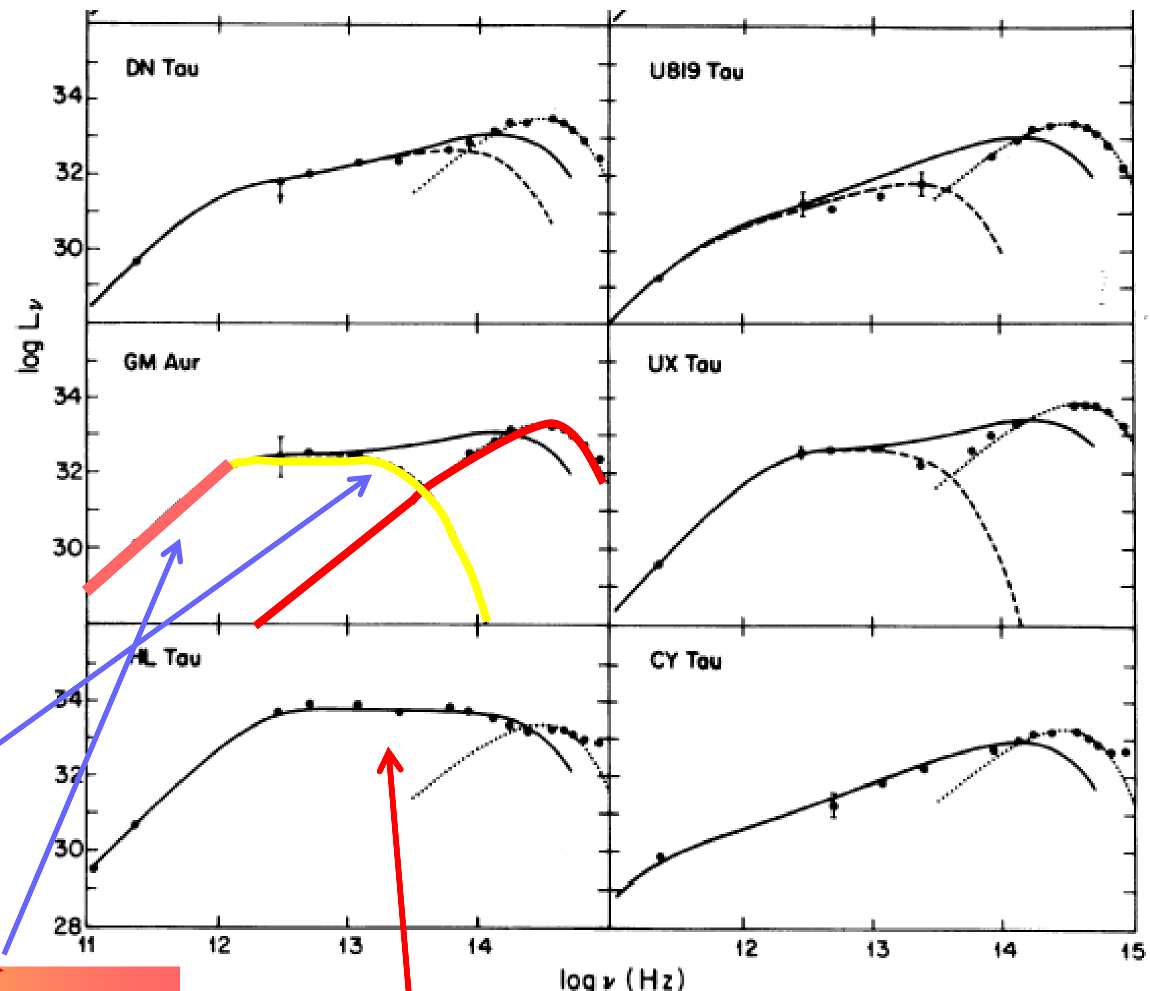

振動数

中心星＋円盤

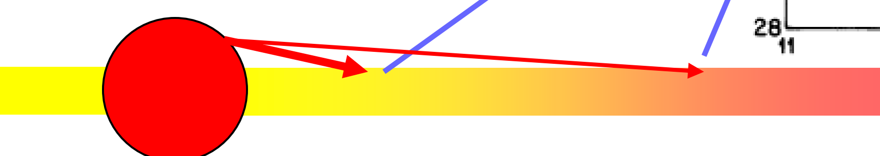

高温
高振動数

低温
低振動数

フラットスペクトル
Tタウリ型星

ディスク・ハロー モデル

ハロー：エンベロープの
内側100 AU程度の領域

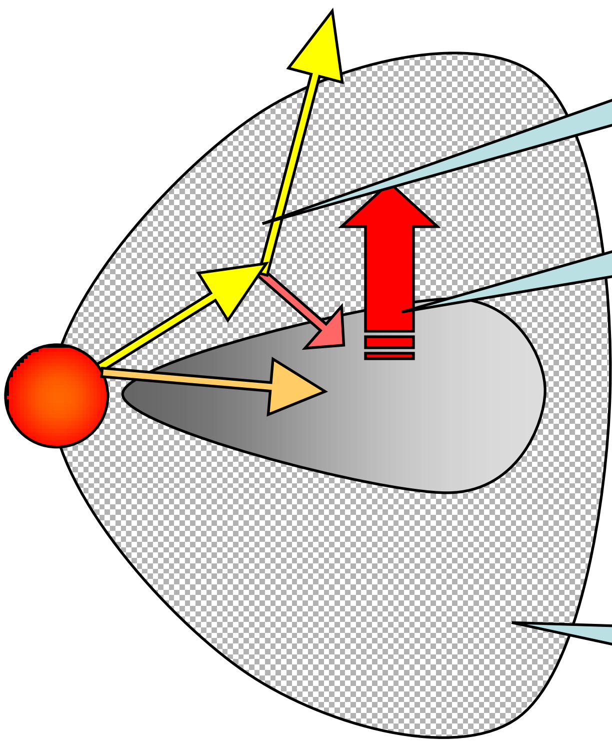

中心星の放射を
エンベロープが散乱

加熱されたディスク
からの赤外放射

中心星からの放射を直接吸収
するよりも多くの輻射を吸収する

エンベロープはディスクからの
赤外放射に対して光学的薄い

基礎方程式

１. 輻射輸送方程式：輻射によるエネルギー輸送を記述

$$\frac{dI_\nu}{ds} = \underbrace{-\chi_\nu^{abs} I_\nu}_{\text{吸収}} + \underbrace{\chi_\nu^{abs} B_\nu}_{\text{放射}} \underbrace{- \chi_\nu^{sca} I_\nu + \chi_\nu^{sca} \frac{1}{4\pi} \oint I_\nu d\Omega}_{\text{散乱}}$$

２. 輻射平衡：物質の温度分布を決定

$$\underbrace{\int_0^\infty \chi_\nu^{abs} B_\nu d\nu}_{\text{放射}} = \underbrace{\int_0^\infty \chi_\nu^{abs} J_\nu d\nu}_{\text{吸収}}$$

I_ν ：輻射強度　　　χ_ν^{abs} ：吸収係数

B_ν ：プランク関数　χ_ν^{sca} ：散乱係数

J_ν ：平均輻射強度

2D 輻射平衡計算

T Tauri型星 HL Tau

・2次元 軸対称
・輻射平衡，VEF

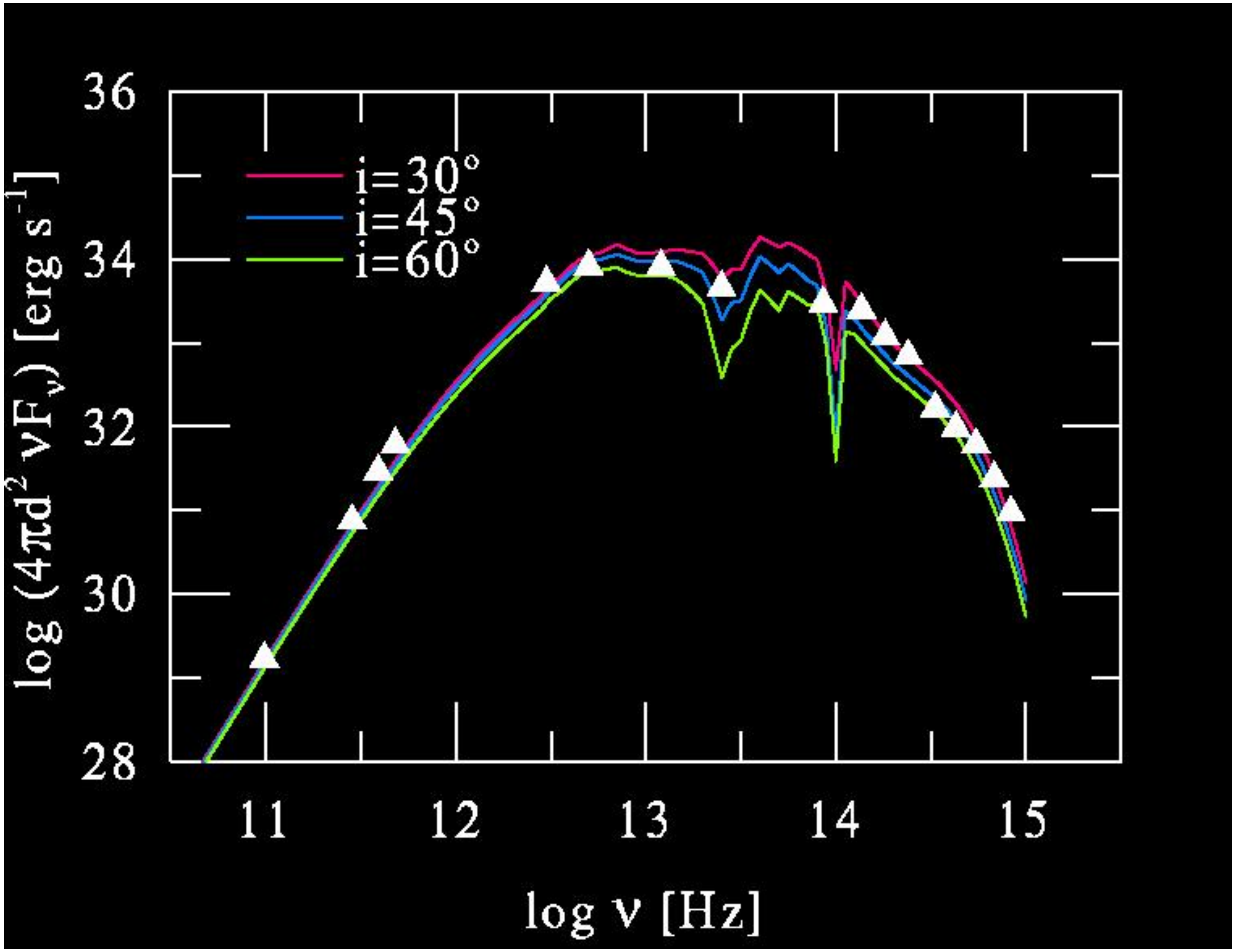

Kikuchi, Nakamoto, & Ogochi 2002

密度・温度分布

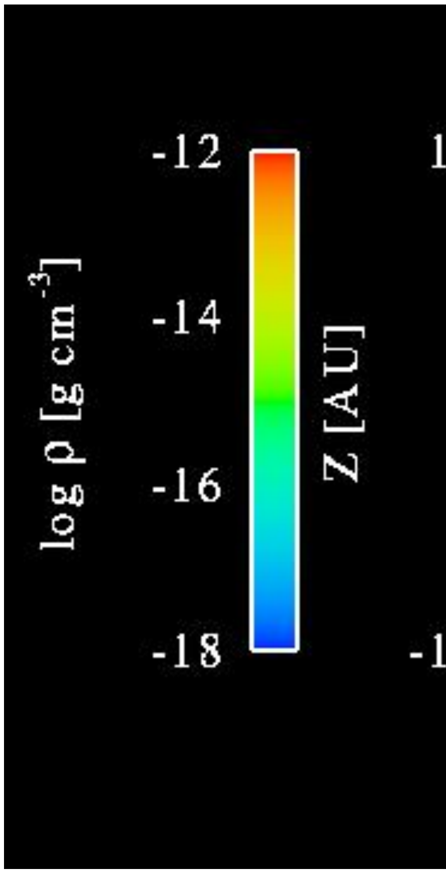
log ρ [g cm^-3]
-12
-14
-16
-18
Z [AU]

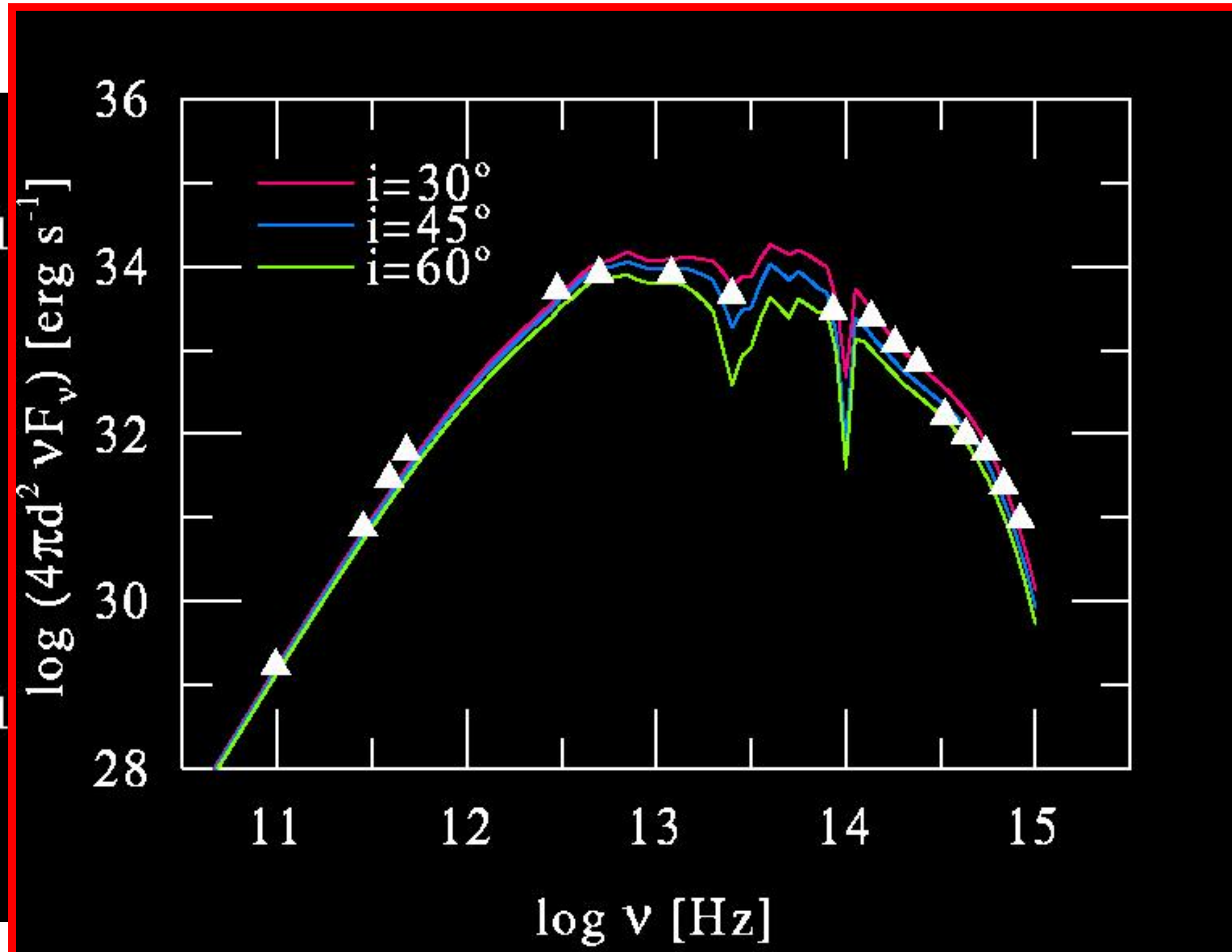
i=30°
i=45°
i=60°
log (4πd² νF_ν) [erg s^-1]
log ν [Hz]
36
34
32
30
28
11
12
13
14
15

近赤外散乱光イメージ

観測 (HL Tau)

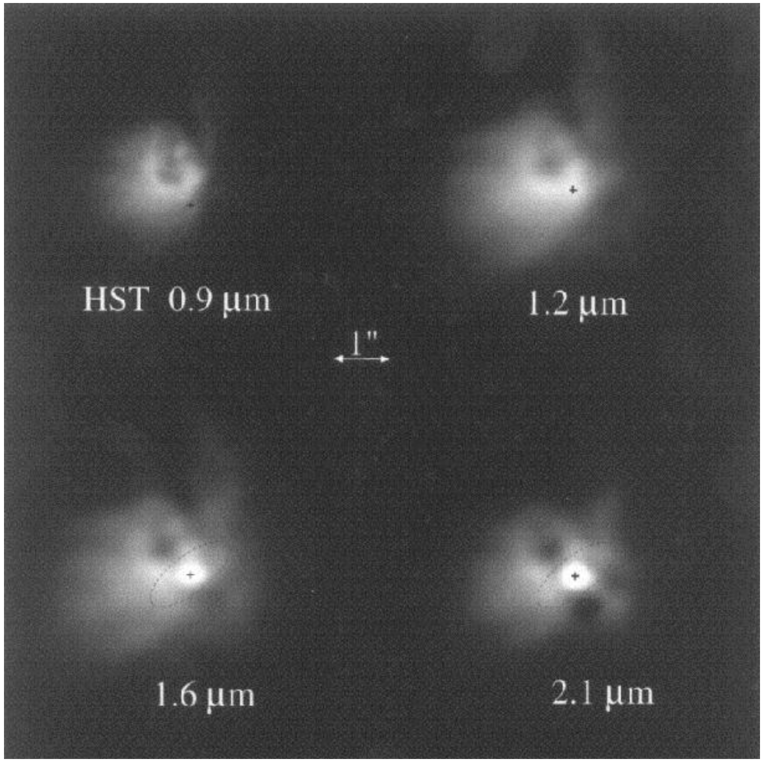

Close et al. (1997)

モデル計算 (i = 60^{o})

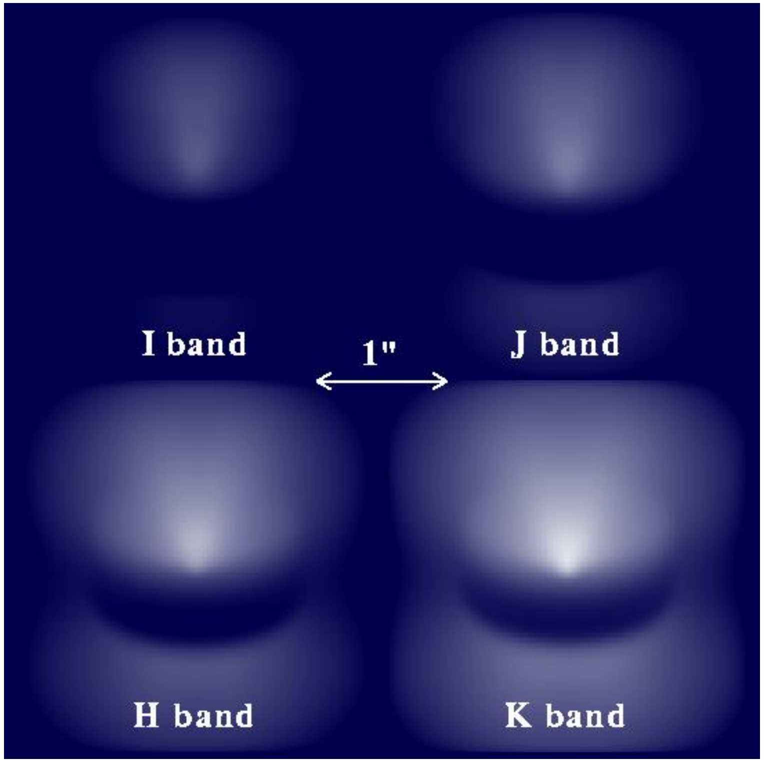

参考文献

- André, P., Men’shchikov,A., Bontemps,S. et al., 2010: From filamentary clouds to prestellar cores to the stellar IMF : Initial highlights from the Herschel Gould Belt Survey, Astronomy and Astrophysics,518 : p. L102.
- André, P. et al. 2002: Molecular line study of the very young protostar IRAM 04191 in Taurus: infall, rotation, and outflow, Astronomy and Astrophysics, v.393, p.927-947
- BO REIPURTH, DAVID JEWITT, AND KLAUS KEIL, (Lori Allen, S.Thomas Megeath, Robert Gutermuth, Philip C. Myers, Scott Wolk, Fred C. Adams , James Muzerolle, Erick Young, Judith L. Pipher) 2007: Protostars and Planets V(The Structure and Evolution of Young Stellar Clusters), The University of Arizona Press pp683 (pp361)
- Beckwith, Steven V. W et al. 1990: A survey for circumstellar disks around young stellar objects, Astronomical Journal, vol. 99, p. 924-945
- Baba Junichi et al. 2009: The Origin of Large Peculiar Motions of Star-Forming Regions and Spiral Structures of Our Galaxy, The Astrophysical Journal, vol. 706, no. 1, pp. 471-481

参考文献

- Fiebig, D. et al. 1989: Strong magnetic fields in interstellar H2O maser clumps, Astronomy and Astrophysics, vol. 214, no. 1-2, April 1989, p. 333-338.
- Goodman, A. et al. 1993: Dense cores in dark clouds. VIII - Velocity gradientsAstrophysical Journal, vol. 406, p. 528-547.
- Inutsuka, Shu-Ichiro; Miyama, Shoken M. 1992: Self-similar solutions and the stability of collapsing isothermal filamentsAstrophysical Journal, vol. 388, p. 392-399.
- Kikuchi, Nobuhiro; Nakamoto, Taishi; Ogochi, Koji 2002: Disk-Halo Model for Flat-Spectrum T Tauri Stars, Publications of the Astronomical Society of Japan, Vol.54, No.4, pp.589-597
- Kemper, F, Vriend, W. J, Tielens, A. G. G. M 2004: The Absence of Crystalline Silicates in the Diffuse Interstellar Medium, The Astrophysical Journal, Volume 609, Issue 2, pp. 826-837
- Charles J. Lada & Elizabeth A. Lada 2003: Embedded Clusters in Molecular Clouds , Annual Reviews of Astronomy and Astrophysics, Vol. 41, pg. 57.
- Larson, R. B. 1969: Numerical calculations of the dynamics of collapsing proto-star Monthly Notices of the Royal Astronomical Society, Vol. 145, p.271

参考文献

- F. J. Molster, et al. 2001: IRAS 09425−6040: A carbon star surrounded by highly crystalline silicate dust, Astronomy&Astrophysics, 366, pp.923-929
- 松田准一 ,圦本尚義 2008: 宇宙・惑星化学 (地球化学講座2), 培風館 pp.291
- Masunaga, Hirohiko; Miyama, Shoken M.; Inutsuka, Shu-Ichiro1998: A Radiation Hydrodynamic Model for Protostellar Collapse. I. The First Collapse , Astrophysical Journal v.495, p.346
- S . Matsuura et al. 2011: DETECTION OF THE COSMIC FAR-INFRARED BACKGROUND IN AKARI DEEP FIELD SOUTH The Astrophysical Journal, 737:2 (19pp)
- Mathewson, D. S.; Ford, V. L. 1970: Polarization observations of 1800 stars, Mem. R. Astron. Soc., 74, 139
- Mathis, J. S, Rumpl, W, Nordsieck, K. H, 1977: The size distribution of interstellar grains, Astrophysical Journal, Part 1, vol. 217, p. 425-433.

参考文献

- Tomoaki Matsumoto; and Tomoyuki Hanawa 2003: FRAGMENTATION OF A MOLECULAR CLOUD CORE VERSUS FRAGMENTATION OF THE MASSIVE PROTOPLANETARY DISK IN THE MAIN ACCRETION PHASE The Astrophysical Journal, 595:913–934
- Tomoaki Matsumoto and Kohji Tomisaka 2004: Directions of Outflows, Disks, Magnetic Fields, and Rotation of Young Stellar Objects in Collapsing Molecular Cloud Cores, The Astrophysical Journal, 616:266-282
- Takeshi Nakazato , Taishi Nakamoto , and Masayuki Umemura 2003: A Spectrophotometric Method to Determine the Inclination of Class I Objects, The Astrophysical Journal, 583:322-329

参考文献

- Sakamoto, Seiichi; Hayashi, Masahiko; Hasegawa, Tetsuo; Handa, Toshihiro; Oka, Tomoharu 1994: A large area CO (J = 2 goes to 1) mapping of the giant molecular clouds in Orion, The Astrophysical Journal, vol. 425, no. 2, pp. 641-652
- Toru Tsuribe and Shu-ichiro Inutsuka 1999: Criteria for Fragmentation of Rotating Isothermal Clouds Revisited, The Astrophysical Journal, 523:L155-L158
- Troland, T. H. & Heiles, C. 1986: Interstellar magnetic field strengths and gas densities Observational and theoretical perspectives, Astrophysical Journal, vol. 301, Feb. 1, 1986, pp. 339-345
- Zhi-Yun Li and Fumitaka Nakamura 2004: Magnetically Regulated Star Formation in Turbulent Clouds , The Astrophysical Journal, 609:L83-L86